Unconventional Resources 8 (2025) 100247

Contents lists available at ScienceDirect

Unconventional Resources

journal homepage: www.keaipublishing.com/en/journals/unconventional-resources/

Pore structure and gas content evaluation of coal-rock gas using well log data

Fei Zhao [a,b], Jin Lai [a,b,*], Lu Xiao [a,b], Zongli Xia [a,b], Zhongrui Wang [a,b], Ling Li [c], Bin Wang [c], Guiwen Wang [a,b]

[a] National Key Laboratory of Petroleum Resources and Engineering, China University of Petroleum (Beijing), Beijing, 102249, China
[b] College of Geosciences, China University of Petroleum (Beijing), Beijing, 102249, China
[c] Research Institute of Petroleum Exploration and Development, Tarim Oilfield Company, CNPC, Korla, Xinjiang, 841000, China

ARTICLE INFO

Keywords:
Coal-rock gas
Pore structure
Fractal dimension
Gas bearing property
Well log
Low-medium rank coal

ABSTRACT

The pore structure of coal significantly affects the adsorbability, desorption, and seepage behavior of coal-rock gas. This study firstly represents a comprehensive assessment of pore structure and fractal dimension characteristics for the low-medium rank coal of the Jurassic-Triassic, Kuqa Depression, Tarim Basin, China, with a focus on their implications for methane adsorption capacity. In addition, integration the laboratory and well log data (CMR_NG) are used to evaluate gas bearing property of coal seams. Coal samples of low-medium rank were analyzed using low-pressure CO_2 adsorption (LP-CO_2GA), low-temperature N_2 adsorption (LT-N_2GA), mercury intrusion porosimetry (MIP), nuclear magnetic resonance (NMR), and scanning electron microscopy (SEM). The adsorption-desorption isotherms of coal samples are predominantly Type H3 and H4, indicating parallel plate pores and ink-bottle or narrow slit pores, which promote coal-rock gas enrichment. Micropores, responsible for most specific surface area (SSA), dominate the pore structure, alongside macropores with two T_2 peaks. Fractal dimensions (D_1, D_2 from LT-N_2GA; D_3, D_4 from NMR) reflect pore characteristics, where higher D_1 and D_2 correlate positively with SSA and total pore volume (TPV) of micropores and mesopores. Langmuir volume (V_L) correlates with D_3, indicating greater adsorption capacity, while lower D_4 suggests better connectivity and permeability. Furthermore, industrial components and gas bearing property are evaluated by using conventional well log and CMR_NG log. The favorable coal reservoir exhibits high fixed carbon content, a broad T_1 spectrum, and bimodal T_2 distributions from CMR_NG, indicating both adsorbed and free gas with high coal-rock gas content. These insights could enhance understanding of low-medium rank coal reservoir pore structure and fractal dimension characteristics, as well as their influence on methane adsorption, gas bearing property and seepage capacity.

1. Introduction

Despite the ongoing energy transition, fossil fuels, particularly oil and gas, are expected to remain dominant in the energy sector for the coming decades [1,2]. Coal, as a substance with a porous nature, exhibits a complex and heterogeneous pore structure that significantly affects its capacity for methane adsorption and seepage [3–6]. Generally, the study of pore size distribution (PSD) is used to characterize the pore structure of coal reservoirs [7,8]. Pore volume (PV), specific surface area (SSA), connectivity, and pore types are crucial for determining the storage and transportation mechanisms of coalbed methane (CBM) [9,10]. In addition, the gas adsorption mechanism is believed to be influenced by PSD and SSA as vital factors [11,12]. There are various pore classification schemes, including the Hodot system and the IUPAC system, which have been widely used [13,14]. The adsorption and seepage capabilities of coal are greatly influenced by various kinds of pore types. Micropores and transition pores, also known as adsorption pores, are of great significance for gas adsorption and storage [10,15,16]. The adsorption capacity of coal is closely linked to micropore development [9,17,18]. Conversely, mesopores and macropores hold significant roles in seepage pores and are typically considered the primary pathways for CBM [19,20]. Thus, the methane adsorbability and

Peer review under the responsibility of KeAi Communications Co., Ltd.
* Corresponding author. National Key Laboratory of Petroleum Resources and Engineering, China University of Petroleum (Beijing), Beijing, 102249, China.
E-mail address: laijin@cup.edu.cn (J. Lai).

https://doi.org/10.1016/j.uncres.2025.100247
Received 21 July 2025; Received in revised form 7 September 2025; Accepted 19 September 2025
Available online 19 September 2025

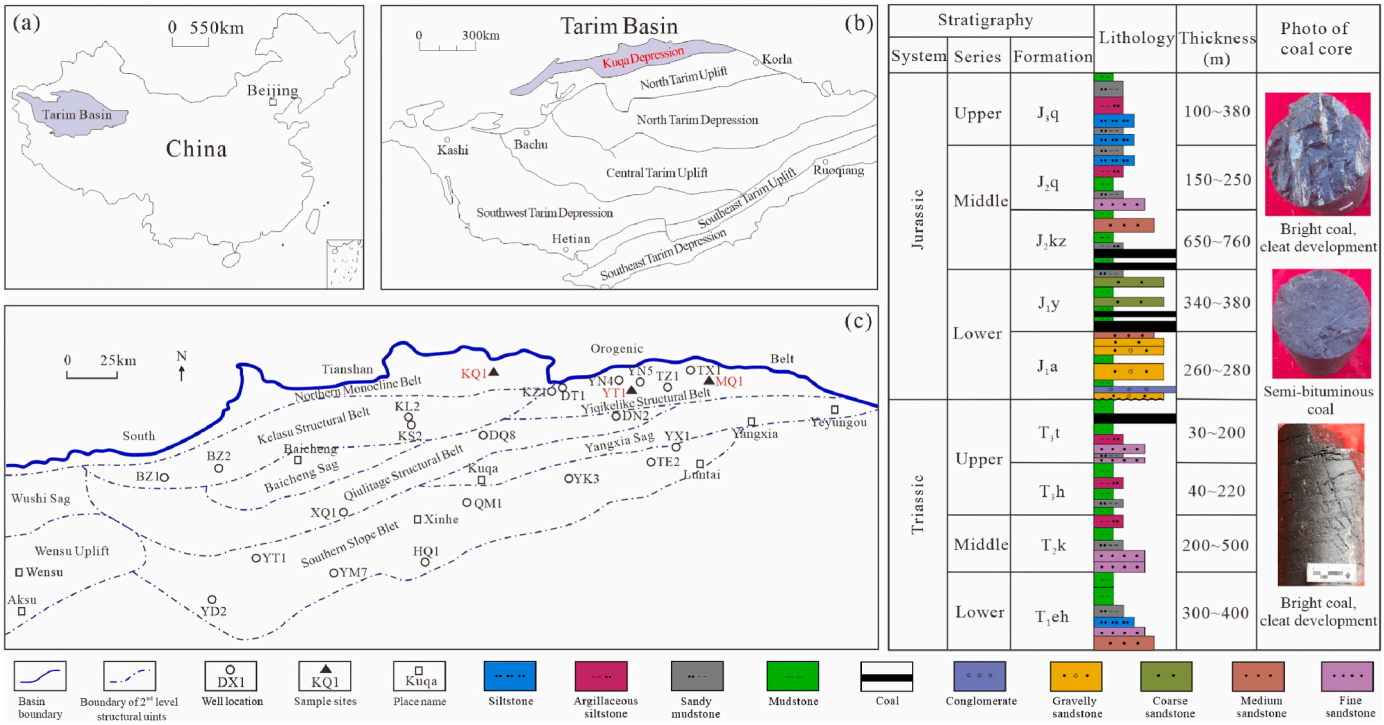

Fig. 1. Location, geological structures and stratigraphic column. **(a, b)** location of the Tarim Basin in China. **(c)** location of the study area and the distribution of coal samples in the Kuqa Depression.

Table 1
Proximate analysis, Ro and CH_4 isothermal adsorption experiments results.

Sample number	Formation	Proximate analysis (%)				CH_4 isothermal adsorption		
		Mad	Aad	Vad	Fcad	V_L (m^3/t)	P_L (MPa)	Ro (%)
KQ1	T3t	1.69	3.39	39.04	55.89	14.02	3.65	0.58
KQ3	T_3t	1.63	28.66	25.55	44.17	/	/	0.69
KQ2	T_3t	1.15	7.04	31.56	60.26	16.46	3.41	0.72
KQ4	T_3t	1.11	3.52	37.23	58.15	/	/	0.66
KQ5	T_3t	1.19	5.12	34.24	59.46	18.29	2.15	0.69
MQ1	J_2kz	3.14	1.24	28.76	66.86	11.05	4.51	0.44
MQ2	J_2kz	3.07	1.30	26.08	69.55	11.60	4.74	0.65
MQ3	J_2kz	3.13	11.83	32.77	52.27	12.51	5.04	0.60
YT1	J_2kz	1.14	3.79	25.38	69.69	12.11	3.06	0.82
YT2	J_2kz	1.82	1.92	28.16	68.10	12.14	3.23	0.83

Mad, moisture content on air-dried basis; Aad, ash yield on dried basis; Vad, volatile yield on dry ash-free basis; Fcad, fixed carbon content on air-dried basis; V_L, Langmuir volume; P_L, Langmuir volume; Ro, average random reflectance of vitrinite.

seepage capacity of coal reservoirs are closely related to their pore structure [21,22]. Various pore types with different apertures play different parts in the enrichment and development of CBM [4,10].

Currently, deep coal-rock gas has been exploited successfully in the Ordos Basins in China, primarily focusing on high-rank coal [23,24]. Little study is performed on the low-medium rank coal and associated coal-rock gas, thus, it is crucial to understand the characteristics of pore structures due to the significant potential of low-medium rank coal reservoir [4,9,25]. Revealing the distribution of pore structures in coal and its influence on methane adsorption is the main objective [20,26]. It is challenging to accurately and statistically characterize pore size distribution across multi-scales using a single method [25].

There are mainly three techniques currently used for the study of coal pore structures, including fluid injection, image analysis and physical detection [8,14]. The method of fluid injection is employed to evaluate porous media that contain non-wetting fluids, and the relevant parameters of pore structure can be computed correspondingly [12,16,20,27]. Image analysis techniques like scanning electron microscopy (SEM), are used to observe the morphology, size and distribution of pores [28]. Qualitative and quantitative evaluations of multi-scale pore spaces in coal reservoirs can be provided by physical detection approaches such as computed tomography (CT) [29,30]. It's important to note that every technology comes with its own distinct strengths and limitations. Therefore, integration of these three technologies provides a comprehensive understanding of pore structure, reflecting its intrinsic characteristics [14,25]. In addition, fractal theory is also useful for depicting the complexity and irregularity of the coal pore structure, enhancing our understanding of the physical attributes of complex pore-fracture systems both on the surface and within coal, as well as the occurrence characteristics of CBM [15,21,23,31].

Geophysical well log data offer high-resolution, vertically continuous insights into the formation, including lithology, fluids, and pore structure [32,33]. Numerous studies have used logging data to evaluate pore structure of sandstone, carbonate rocks, and unconventional shale reservoirs [27,34]. In the realm of coal research, logging data is primarily utilized for determining physical parameters and industrial components of coal, assessing coal strength, and coal texture [35,36]. Nevertheless, there remains limited studies on the pore structure and gas

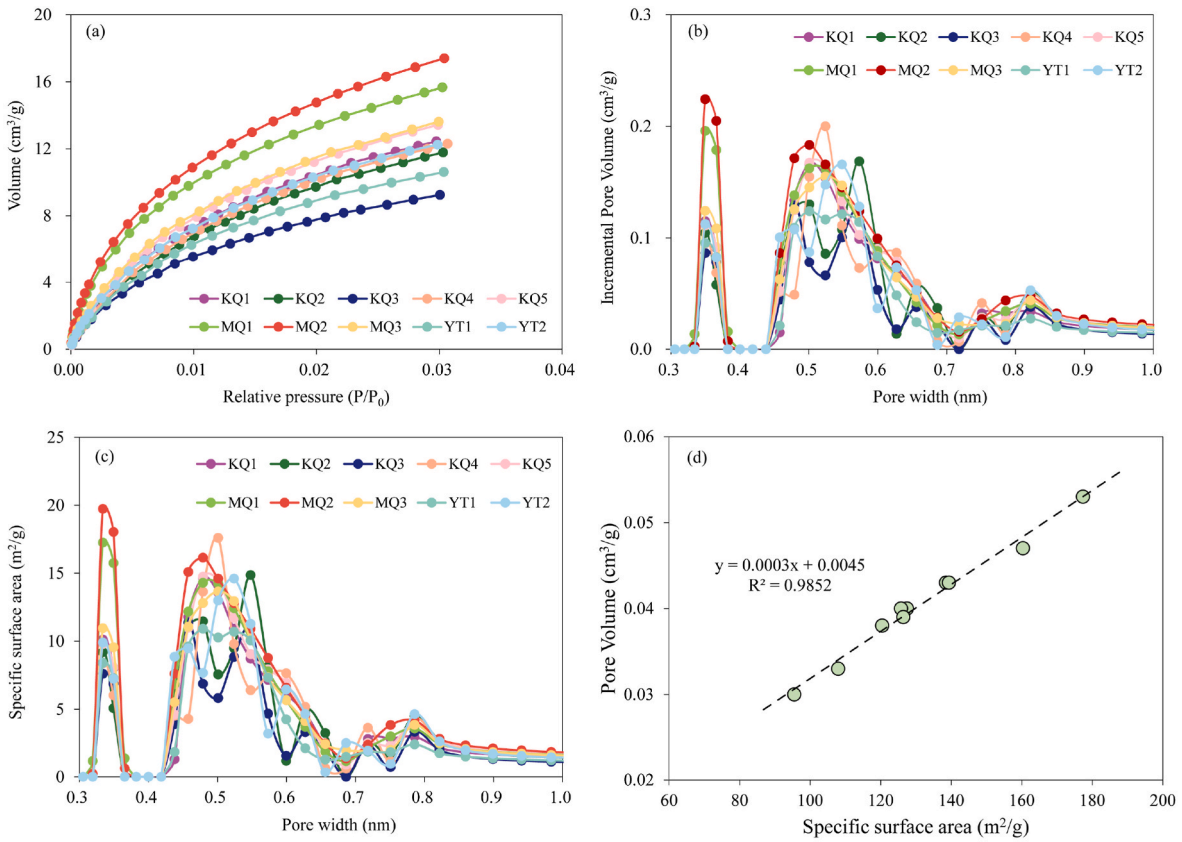

Fig. 2. PSD characteristics of the low-medium rank coal samples based on the LP-CO_2GA. **(a)** CO_2 adsorption isotherms; **(b) (c)** pore volume and specific surface area distribution characteristics of the coal samples based on the LT-CO_2GA experiment, respectively; **(d)** the relationship between specific surface area and pore volume.

bearing property of coal using geophysical well logs, with the aim to provide continuous evaluation of coal reservoir. Deep coal-rock gas holds substantial resource potential; however, pore-structure characterization and assessment of gas-bearing capacity remain limited [37,38]. Furthermore, evaluation frameworks that integrate microscale pore-structure of coal samples with macroscale gas-bearing capacity of coal seams are lacking, which constrains the optimal selection of target intervals for hydraulic-fracturing in deep coal seams.

This study firstly aims to comprehensively analysis the pore structure and fractal dimension of low-medium rank coal and their implications on methane adsorption and seepage in Jurassic to Triassic coal samples from the Kuqa Depression, Tarim Basin, China. Full-scale pore structure is characterized by using the LP - CO_2GA, LT - N_2GA, MIP, NMR and SEM test methods, and fractal dimension is calculated with LT - N_2GA and NMR data. In addition, geophysical well log data are utilized to calculate the industrial components and total gas content, and integrated Schlumberger's CMR_NG logging data to analyze the factors influencing gas content in coal. The findings will enhance to a better understanding of coal-rock gas potential in low-medium rank coal, and have significant implications for exploring and developing coal-rock gas resources with similar geological settings.

2. Geological settings

In the northwest of China lies the Tarim Basin, with the Kunlun-Altun Mountains to its south and the Southern Tianshan Mountains to its north as its boundaries [39]. In the northern part of the Tarim Basin lies the Kuqa Depression, which is a foreland depression that took shape from the Mesozoic to the Cenozoic (Fig. 1a and b). The study area, situated in the northern Tarim Basin, is characterized as a foreland depression formed during the Mesozoic to Cenozoic eras [40]. In the Mesozoic era, it functioned as a continental lacustrine basin characterized by a lake-river-delta sedimentary systems, containing interbedded conglomerates, sandstones, siltstones, mudstones, and coal layers [41]. During the Mesozoic time of the Kuqa Depression, five distinct sets of thick source rocks are deposited [40,41]. The T_3t, J_1y, and J_2kz Formations are identified as coal-bearing source rocks, whereas the T_3h, and J_3q formations are recognized as lacustrine source rocks [42]. Notably, extensive coal-bearing strata can be observed within the T_3t, J_1y and J_2kz Formations [43,44].

3. Samples and methods

3.1. Experiments and methods

The samples utilized in this research were obtained from coal-bearing drilling cores originating from both the Kezilenuer and the Taliqike Formation extracted from three wells within the Kuqa Depression (Fig. 1). During the drilling of well YT1, the coal seam of Kezilenuer Formation was encountered at a depth exceeding 4000 m.

Vitrinite reflectance (50 testing points, oil immersion) was measured followed SY/T 5124-2012, and proximate analysis followed GB/T 212–2008 (Table 1).

Pore structure was characterized by integrating LP-CO_2 and LT-N_2 gas adsorption, mercury intrusion porosimetry (ISO 15901–1:2005), nuclear magnetic resonance (SY/T 6490-2014), and SEM (GB/T 16594-2008) to span micropores to macropores [15,21]. Ten samples were analyzed by gas adsorption (N_2 at 77 K and CO_2 at 273 K) following SY/T 6154-2019 [12,13]. Cylindrical plugs (2.5 cm diameter, 3–4 cm length) were prepared for NMR and MIP test, respectively; powders were used for adsorption. In addition, high-pressure CH4 adsorption isotherms were obtained on eight samples at 30 °C using 60–80 mesh fractions [42].

Well YT1, being the main deep-coal risk exploration well, has

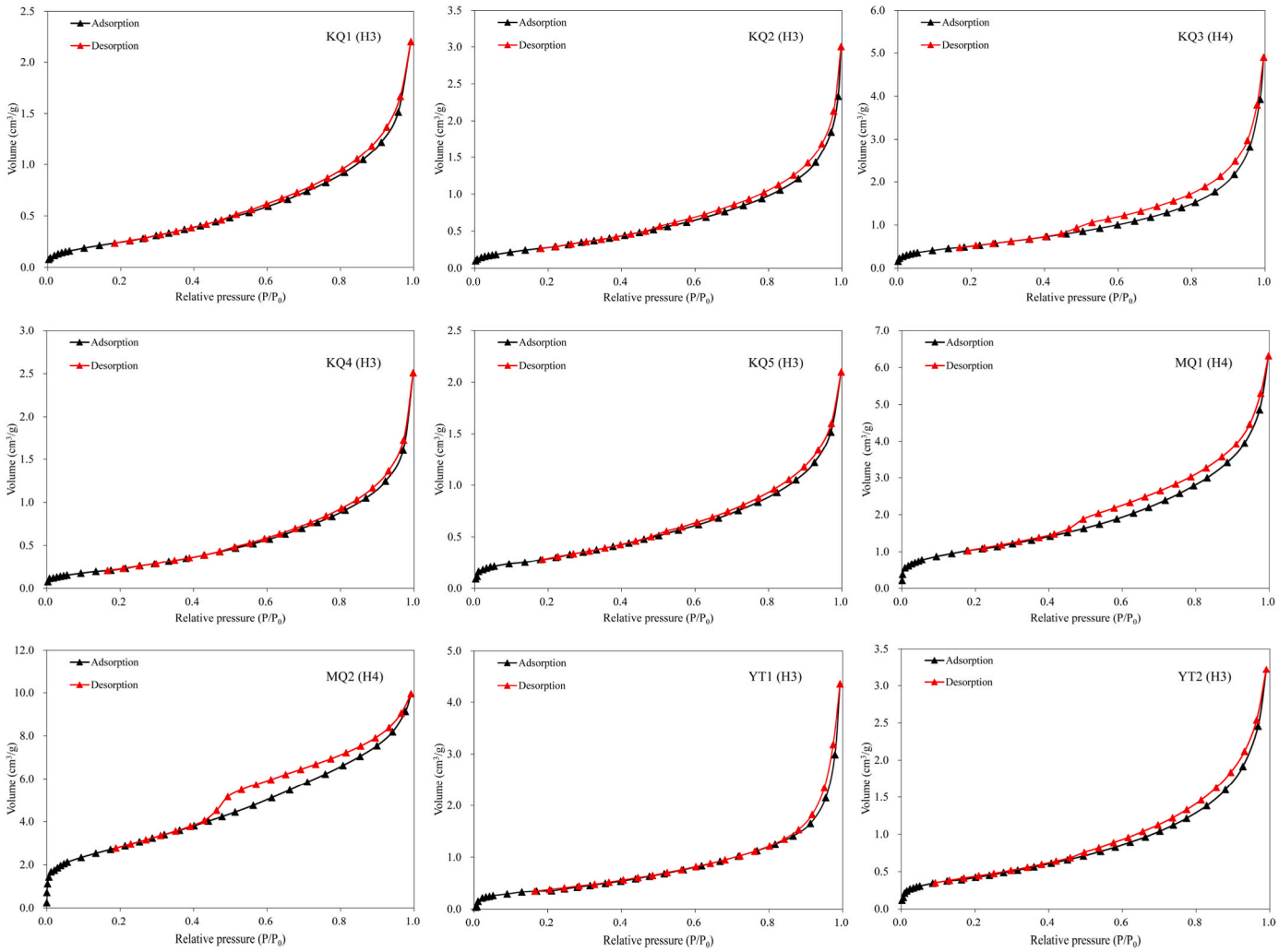

Fig. 3. Nitrogen adsorption-desorption curves of low-medium rank coal samples.

Table 2
The SSA and TPV calculated by LP-CO_2GA and LT-N_2GA of coal samples, the fractal dimensions D_1, D_2, D_3 and D_4.

Samples	Formation	CO_2 adsorption			N_2 adsorption			Fractal dimensions			
		DA-TPV (cm^3/g)	DFT-SSA (m^2/g)	Pore width (nm)	BJH-TPV (cm^3/g)	BET-SSA (m^2/g)	Pore width (nm)	D_1	D_2	D_3	D_4
KQ1	T_3t	0.04	127.509	0.501	0.004	1.463	4.003	2.1680	2.6040	1.3598	2.9556
KQ2	T_3t	0.038	120.472	0.573	0.005	1.621	3.904	2.2423	2.6924	1.3924	2.822
KQ3	T_3t	0.030	95.529	0.479	0.008	2.558	3.747	2.3253	2.6522	0.9955	2.9854
KQ4	T_3t	0.040	125.818	0.524	0.004	1.453	3.968	2.2369	2.7077	1.4815	2.9303
KQ5	T_3t	0.043	138.506	0.501	0.003	1.398	4.06	2.3028	2.6493	1.3472	2.9152
MQ1	J_2kz	0.047	160.340	0.349	0.010	4.322	3.814	2.4509	2.7724	1.0489	2.8653
MQ2	J_2kz	0.053	177.407	0.349	0.0152	10.687	3.843	2.4665	2.8192	1.1498	2.9285
MQ3	J_2kz	0.043	139.385	0.524	0.0078	4.222	3.74	2.4198	2.6926	1.0297	2.8593
YT1	J_2kz	0.033	108.006	0.501	0.0070	1.869	3.122	2.3241	2.5995	1.1270	2.8175
YT2	J_2kz	0.039	126.465	0.548	0.005	2.000	3.843	2.4076	2.6024	1.3573	2.7621

complete log data. It has a set of conventional log data, which consists of caliper (CAL), gamma-ray (GR), induction resistivity logs (M2RX, M2R6 and M2R3), compensated neutron porosity (CNC), acoustic transit time (AC) and bulk density (DEN) logs. In addition, Schlumberger's CMR-MagniPHI (CMR-NG) Combinable Magnetic Resonance logging tool acquired CPMG echo trains at multiple wait times (TW) in the borehole, with a minimum echo spacing of 200μs, a low resonance frequency of 2 MHz in the low magnetism field and a vertical resolution of 22.86 cm. Denoise the measured T_1 and T_2 spectrum to ensure the accuracy of the spectrum information, which obtained continuous T_1 and T_2 spectrum measurements of coal seams.

3.2. *Fractal dimension from low-temperature N_2 adsorption*

The pores of coal are formed during complex process of coalification, resulting in an uneven structure and irregular geometric shapes [22,43]. Consequently, characterizing the pores of coal is challenging. Fractal theory has been proposed to explain the irregularity and highly complex pore structure features, particularly in the complex shale and coal pores found in nature [31].

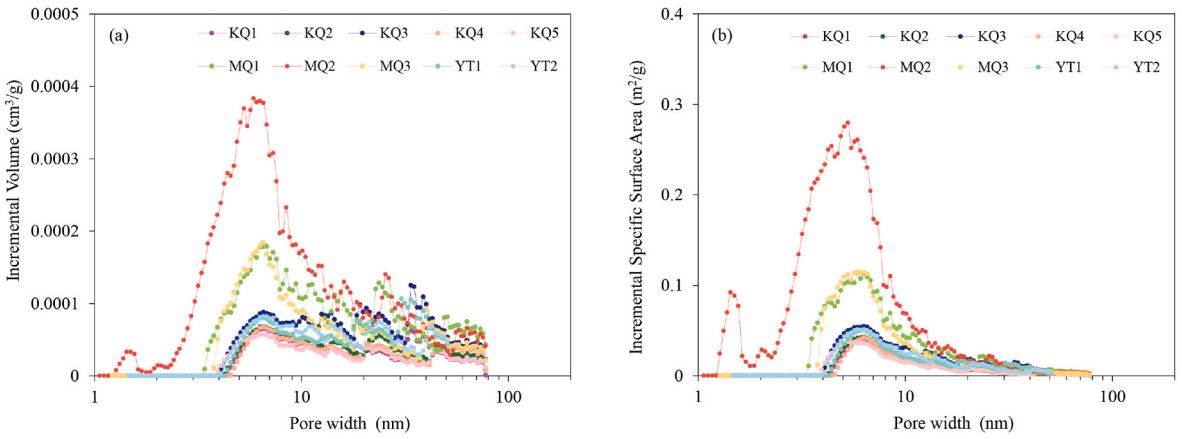

Fig. 4. PSD and SSA distribution characteristics of the coal samples based on the LT-N_2 adsorption.

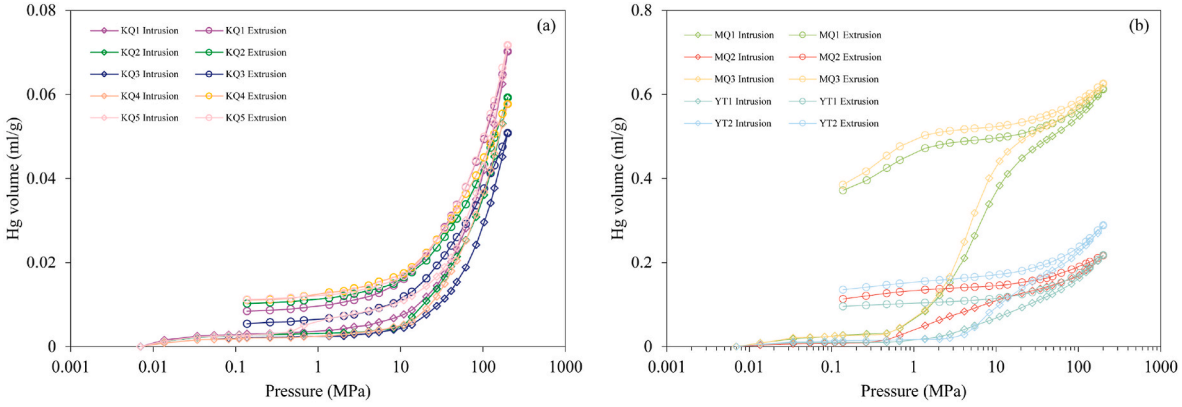

Fig. 5. Mercury intrusion-extrusion curve of coal samples.

The FHH fractal model is a useful method for calculating the fractal dimension of coal pore structure based on gas adsorption isotherms. It has been widely applied in the calculation of fractal dimension in physical adsorption, mainly for the description of multilayer adsorption [45,46]. The FHH model serves to compute the surface fractal dimension of adsorption pores (*D1*), and it can be presented as follows (Eq. (1)):

$$\ln V = A\left[\ln\left(\ln\frac{P_o}{P}\right)\right] + C \tag{1}$$

Where P, Po refers the adsorption equilibrium pressure and the methane gas's saturation pressure, MPa, respectively; V represents the volume of adsorbed gas at the equilibrium pressure, ml; C is a constant; and A is the gradient of the double logarithmic curve plotted as lnV against ln(ln(Po/P)).

Moreover, if the interface is under the control of the surface tension in the liquid - gas system, Eq. (2) can be used to determine the fractal dimension.

$$D = A + 3 \tag{2}$$

The fractal dimension, represented by D, often highlights distinct segmentation in fractal curves, indicating varying fractal properties across two intervals. As a result, two separate fractal dimensions are defined: D_1 for P/P0 < 0.5 and D_2 for P/P0 > 0.5. The roughness of the pore surface is indicated by D_1. A greater D_1 value means that the micropore surface is rougher, which provides more adsorption sites and boosts the methane adsorption capacity. Conversely, D_2 reflects of the pore structure's complexity [9,31].

3.3. Fractal dimension from NMR

It is widely recognized that the MIP method under high-pressure conditions may cause coal matrices to shrink and deform, potentially damaging the pore structure and characterizing connected pores [8,27].

Therefore, the NMR technique has been chosen to determine the fractal dimension. The fundamental theory of NMR fractal geometry and its relation to coal pore structures was expounded by Yao et al. (2010). The NMR fractal model was established for calculating the fractal dimension of adsorption pores and seepage pores, and it can be presented as follows.

$$W = \left[\frac{T_{2\,\max}}{T_2}\right]^{D-3} \tag{3}$$

$$\lg W = (3-D)\lg(T_2) + (D-3)\lg(T_{2\,\max}) \tag{4}$$

Where W represents the portion of accumulated pore volume within the total pore volume, (%); T_2 refers the transverse relaxation time, (ms); D is the pore fractal dimension.

It has been demonstrated in previous studies that NMR can be employed to acquire fractal dimension characteristics of pore structures across various scales [14,21,22]. The fractal dimension D_3 ($T_2 \leq 2.5$ ms), calculated using NMR, can be utilized to characterize adsorption pores, while D_4 ($T_2 > 2.5$ ms) is referred to represent the fractal dimension of seepage pores [14,47].

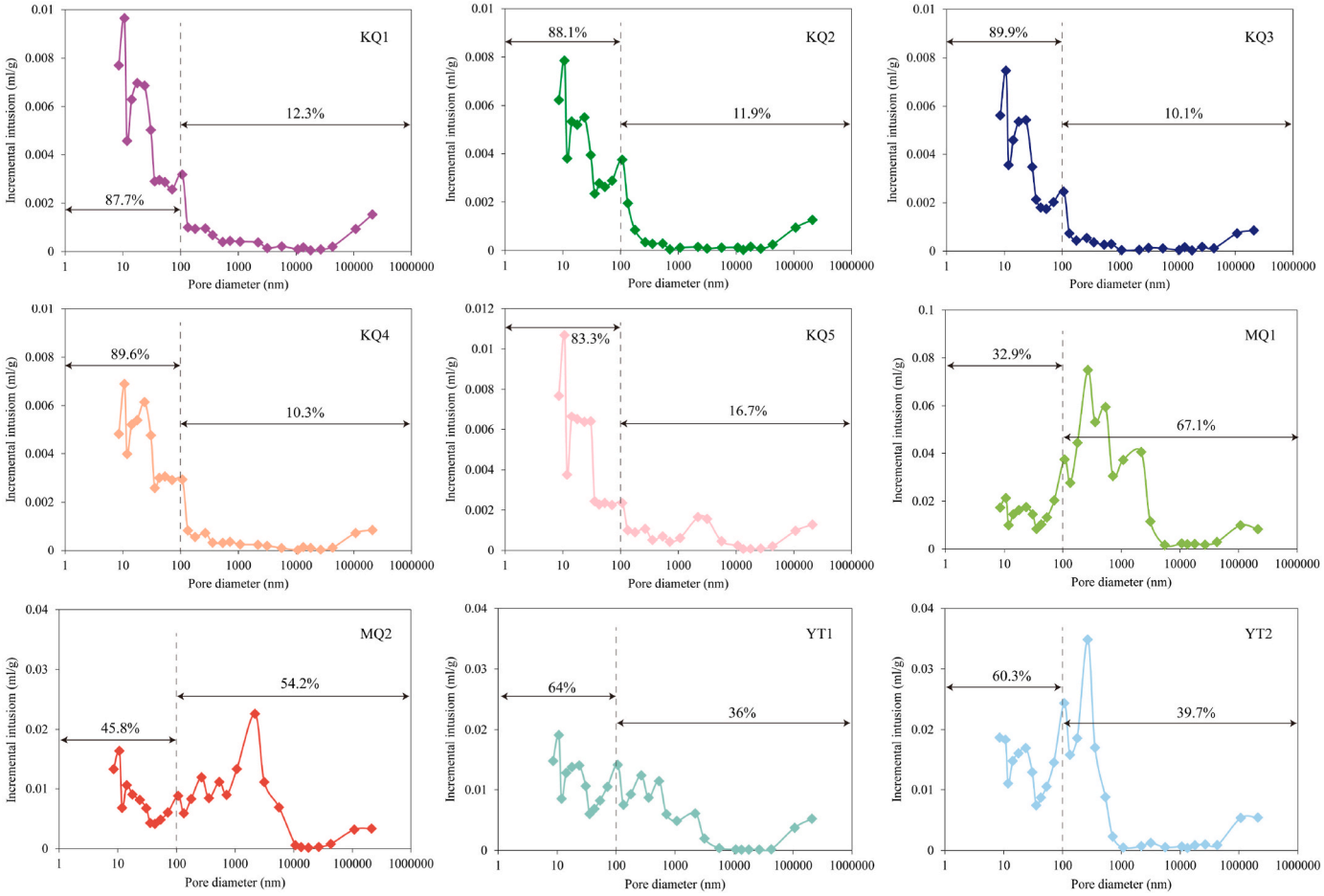

Fig. 6. Pore diameter distribution of coal samples based on MIP.

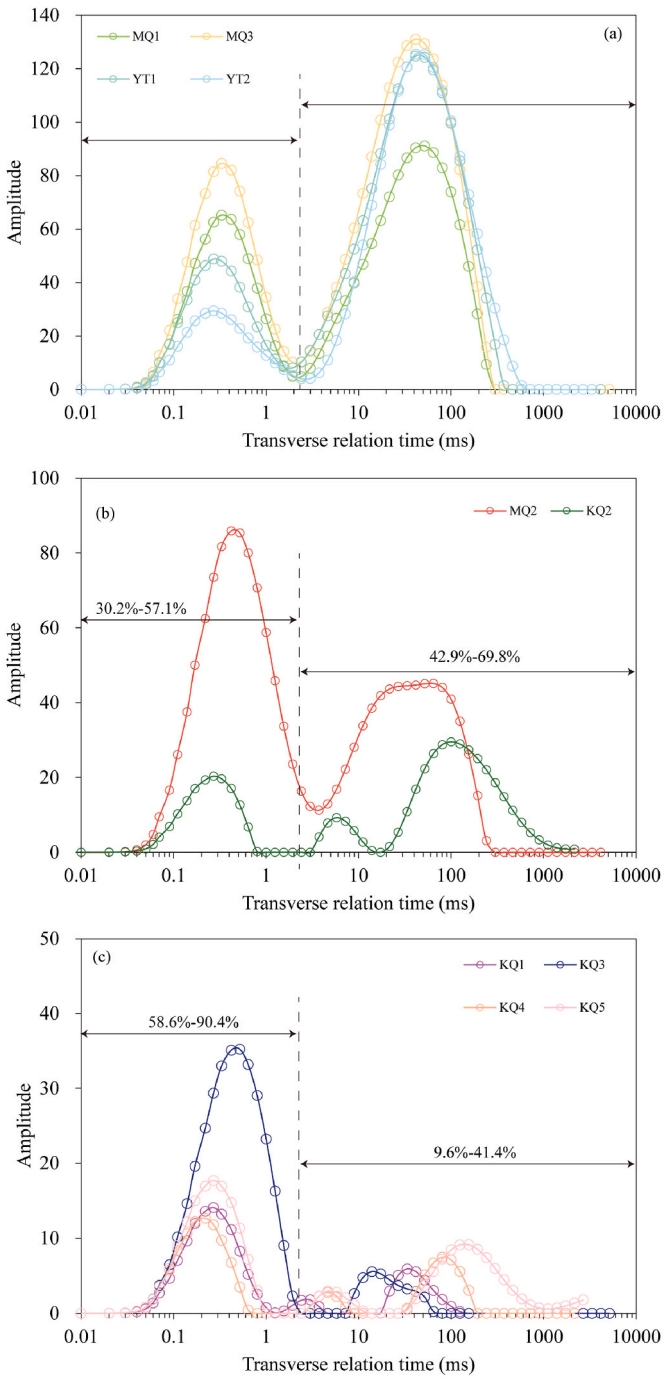

Fig. 7. NMR T_2 distribution of fully saturated-water coal samples.

4. Results

4.1. Pore structure characteristics by LP-CO_2GA

Micropores are pivotal in the adsorption of coalbed methane (CBM), substantially enhancing CH_4 adsorption capacity [4,15]. Generally, a greater SSA of micropores correlates with increased adsorption strength. As can be seen in Fig. 2a, CO_2 adsorption isotherms of coal samples resemble a Langmuir-type profile, characterized by an upward curvature in the low-pressure section, transitioning to a more linear trend as pressure increases. The density functional theory (DFT) and Dubinin-Astakhov (DA) model calculations were used to figure out the CO_2 specific surface area (DFT-SSA) and total pore volume (DA-TPV) for the coal samples [13].

The DFT-SSA ranges from 95.529 to 206.333 m^2/g, while the DA-TPV falls within the range of 0.03–0.059 cm^3/g (Table 1). The pore width distribution of various coal samples reveals consistent patterns, marked by two distinct peaks at 0.3–0.4 nm and 0.45–0.7 nm (Fig. 2b). Additionally, an obvious pore volume can be seen in the range over 0.7 nm. The SSA distribution shows peaks at similar pore width (Fig. 2c). A strong linear correlation is observed between DFT-SSA and DA-TPV (Fig. 2d), indicating that larger surface areas contribute significantly to increased CO_2 adsorption [12].

4.2. Pore structure characteristics by LT-N_2GA

LT-N_2GA experiment is frequently employed to analyze the complexity and morphology of coal pore structure [9,11,46]. Fig. 3 shows the adsorption/desorption isotherms of LT - N_2GA for the coal samples under study. According to the theory of porous material adsorption/condensation, the types of pore shapes can be inferred from the features of LT - N_2GA adsorption/desorption curves. According to the IUPAC classification, the curves for all coal samples exhibit type H3 and H4 characteristics, while H1 and H2 types are absent, indicating the intricate pore structure of coals [8,13].

Type H4, a distinct yield point emerges in the desorption isotherms at a relative pressure (P/Po) of approximately 0.5, suggesting a hysteresis loop primarily attributable to ink-bottle-shaped and narrow slit pores. Type H3, the curves have no clear inflection point when the relative pressure P/P0 = 0.5, and adsorption/desorption isotherms display a narrow hysteresis loop, primarily due to parallel plate pores.

Table 2 illustrates the range of Brunauer-Emmett-Teller (BET) SSA from 1.398 to 10.687 m^2/g, and the Barrett-Joyner-Halenda (BJH) TPV from 0.003 to 0.0152 cm^3/g, which is notably smaller than the results obtained from LP-CO_2 adsorption, indicating a substantial contribution of micropores to the SSA of coal. The PSD and SSA based on nitrogen adsorption tests processed with non-local DFT are depicted in Fig. 4a and b, revealing that the primary peaks of pore size and specific surface area distribution predominantly fall within the range of 4–10 nm. As the pore size increases, the incremental SSA progressively decreases. In addition, it is observed that micropores smaller than 2 nm significantly contribute to the SSA (MQ2), while pores larger than 20 nm make a lesser contribution to the SSA (Fig. 4a).

Table 3
Proximate analysis, test total gas content, lnT_1LM and lnT_2LM from CMR_NG of the deep low-medium rank coals in Tarim Basin.

Sample number	Formation	Proximate analysis (%)				Test total gas content (m^3/t)	lnT_1LM (ms)	lnT_2LM (ms)
		Mad	Aad	Vad	Fcad			
YT1	J_2kz	1.14	3.79	25.38	69.69	12.10	2.97	2.64
YT2	J_2kz	1.82	1.92	28.16	68.10	10.63	1.64	0.94
YT3	J_2kz	1.56	5.20	24.62	68.62	10.90	1.98	1.00
YT4	J_2kz	2.05	4.62	22.28	71.05	11.59	2.13	1.32
YT5	J_2kz	1.32	15.51	27.35	55.82	8.17	1.88	1.11
YT6	J_2kz	4.39	16.54	25.14	53.93	8.44	1.97	1.50
YT7	J_2kz	1.07	26.14	25.05	47.74	6.08	1.35	0.79

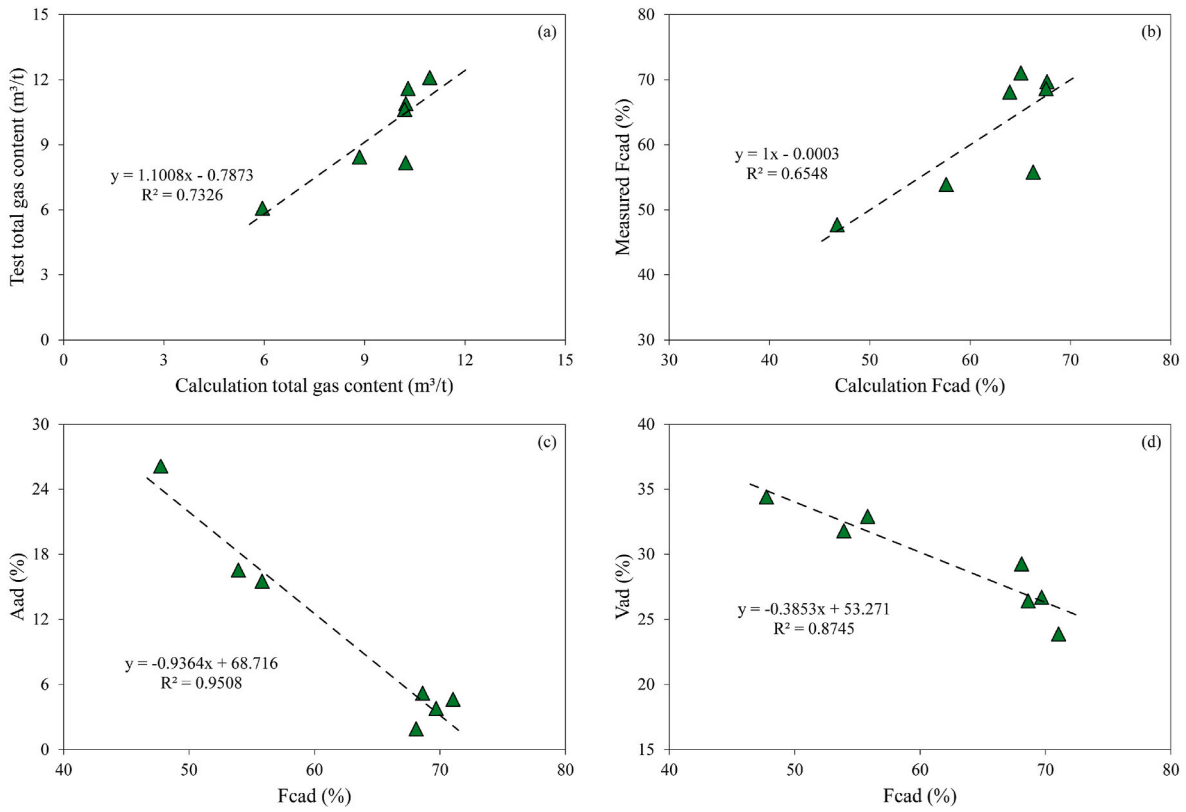

Fig. 8. Total gas content and proximate analysis were calculated using logging data.

4.3. Pore throat distribution by MIP

The pore structure of coal can be directly analyzed through mercury intrusion-extrusion curves, which reveal the features of pore throats as well as the quality of pore connectivity [14]. As is shown in Fig. 5, displays the mercury intrusion-extrusion curves for the coal samples. The high-pressure MIP curve typically exhibits a smooth initial segment followed by a steep rise. In the majority of coal samples, mercury intrusion progresses slowly below 10 MPa, corresponding mainly to macroscopic pores (>100 nm) and indicating that these pores are relatively undeveloped. There is a rapidly increase in mercury intrusion, suggesting the presence of numerous micron and nanoscale pores, upon reaching approximately 10 MPa (Fig. 5a and b). This type curve displays a high volume of micropores and transition pores, limited connectivity, and it facilitates the adsorption of CBM. Conversely, for samples MQ1, MQ2, and MQ3, there are sudden surges in mercury intrusion at around 1 MPa, which are associated with pore throat diameters exceeding 1000 nm, reflecting the development of well-connected macropores (Fig. 5b).

As shown in Fig. 6, the pore diameter distribution is determined by MIP experiment. The pore diameter distribution is in accordance with the curve illustrated in Fig. 5. Pores diameter are predominantly below 100 nm in coal samples of KQ1-KQ5; conversely, samples YT1 and YT2 show a decrease in pores below 100 nm, with a significant increase in those above 100 nm. Meanwhile, samples MQ1-MQ3 primarily exhibit mesoporous (>100 nm) characteristics, along with a certain proportion of micropores and transitional pores.

4.4. Pore size distribution by NMR

NMR can be used to analyze the T_2 relaxation of fully water-saturated coal samples for assessing the distribution and connectivity of pore structures in coal [22]. The T_2 spectrum provides significant insights into the distribution, size, and sorting characteristics of specific pore types [27,49]. Moreover, pore connectivity can be indicated by the continuity of the T_2 spectrum [36]. The seepage pores are associated with the peak of longer relaxation time, and the adsorption pores are related to the peak of shorter relaxation time [14,16].

Both bimodal and triple peaks are observed in T_2 distribution of the coal samples (Fig. 7). All coal samples display adsorption peaks on the left side, with a notable disparity in the intensity of seepage peaks on the right side. The T_2 spectrum can be categorized into three types. The first exhibits a bimodal characteristic, demonstrating strong seepage peaks and relatively robust adsorption peaks, and the relaxation times of the two peaks are approximately 0.3 ms and 40 ms, respectively. A clear transition in pore diameter between the two peaks suggests enhanced pore connectivity and a large portion of seepage pores (Fig. 7a). The second type exhibits an increased proportion of adsorption peaks while retaining a substantial amount of seepage peaks (Fig. 7b). The third type shows distinct adsorption peaks with weaker seepage peak characteristics, dominated by adsorption peaks and poor connectivity between them (Fig. 7c).

4.5. Logging evaluation of total gas content and industrial components

Investigating the impact of pore structure and industrial components on the gas content of deep coal, logging data was utilized to calculate the industrial components and total gas content. The data was obtained from the coal drilling in the Kuqa depression, Tarim Basin, where real-time measurements of total gas content (including lost gas, desorbed gas, and residual gas content) were conducted on site (Table 3). Multiple regression calculations showed a relationship between fixed carbon content and total gas content. The correlation coefficient $R^2 = 0.7326$ between measured gas content and logging calculation results demonstrates strong calculation performance (Fig. 8a). Furthermore, there is a positive correlation between measured industrial components and logging calculation results (Fig. 8b). The calculation formulas can be described as follows (Eq. (5) and (6)).

$$Total\ gas\ content = 4.4875*LnRT - 0.0964*CNC + 4.0661 \quad (5)$$

$$Fix\ carbon\ content = 17.8115*LnRT - 0.7806*CNC + 66.9329 \quad (6)$$

Where *RT* represents the resistivity, *CNC* represents compensated neutron porosity.

Additionally, the strong linear relationship between fixed carbon content and ash as well as volatile matter content indicate that well log data can be used for calculations of ash, volatile matter, and moisture content (Fig. 8c and d).

In Fig. 9, the total gas content and industrial components calculated from well log data are in accordance with the measured results (Fig. 9). Furthermore, as is illustrated in the T_1-T_2 map, a high correlation relationship is observed between the measured total gas content and the

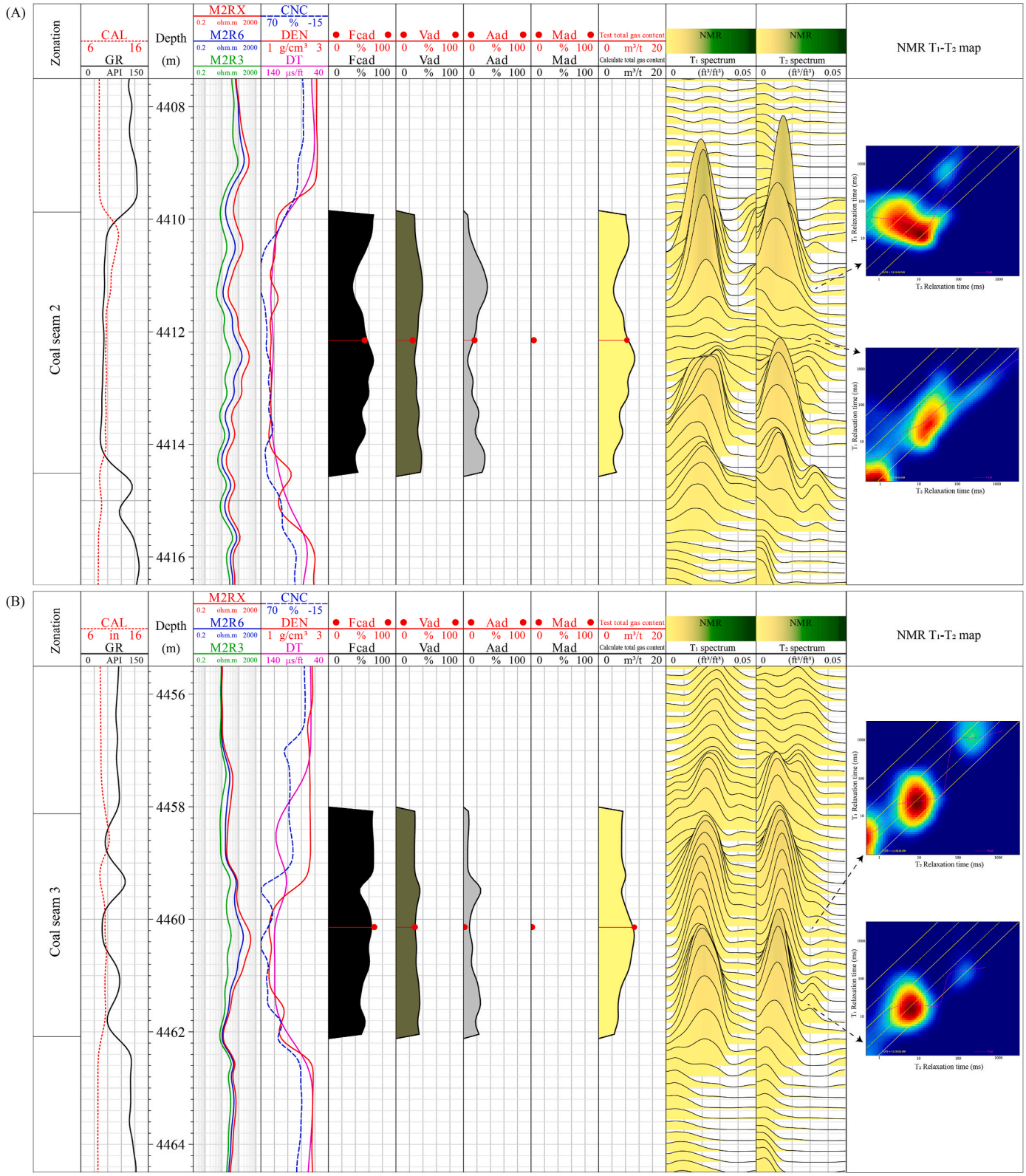

Fig. 9. Logging calculation of total gas content and industrial components of well YT1 in Tarim Basin.

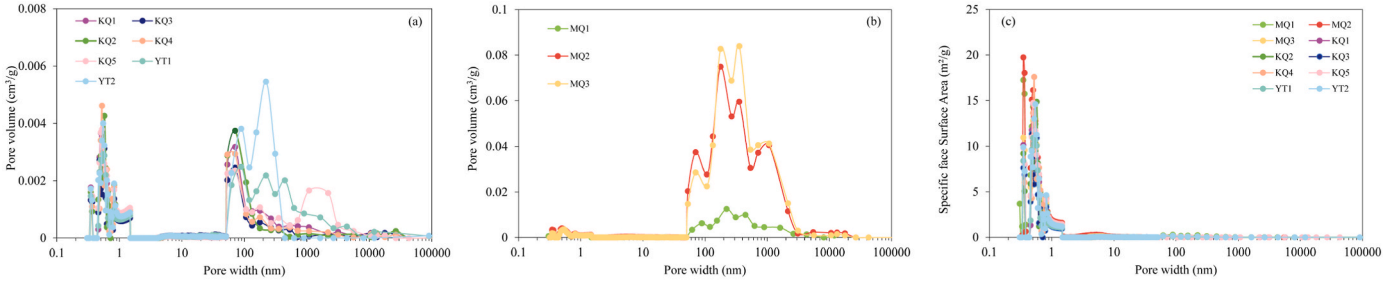

Fig. 10. PSD curves and SSA based on the LP-CO_2GA, LT-N_2GA, and MIP methods.

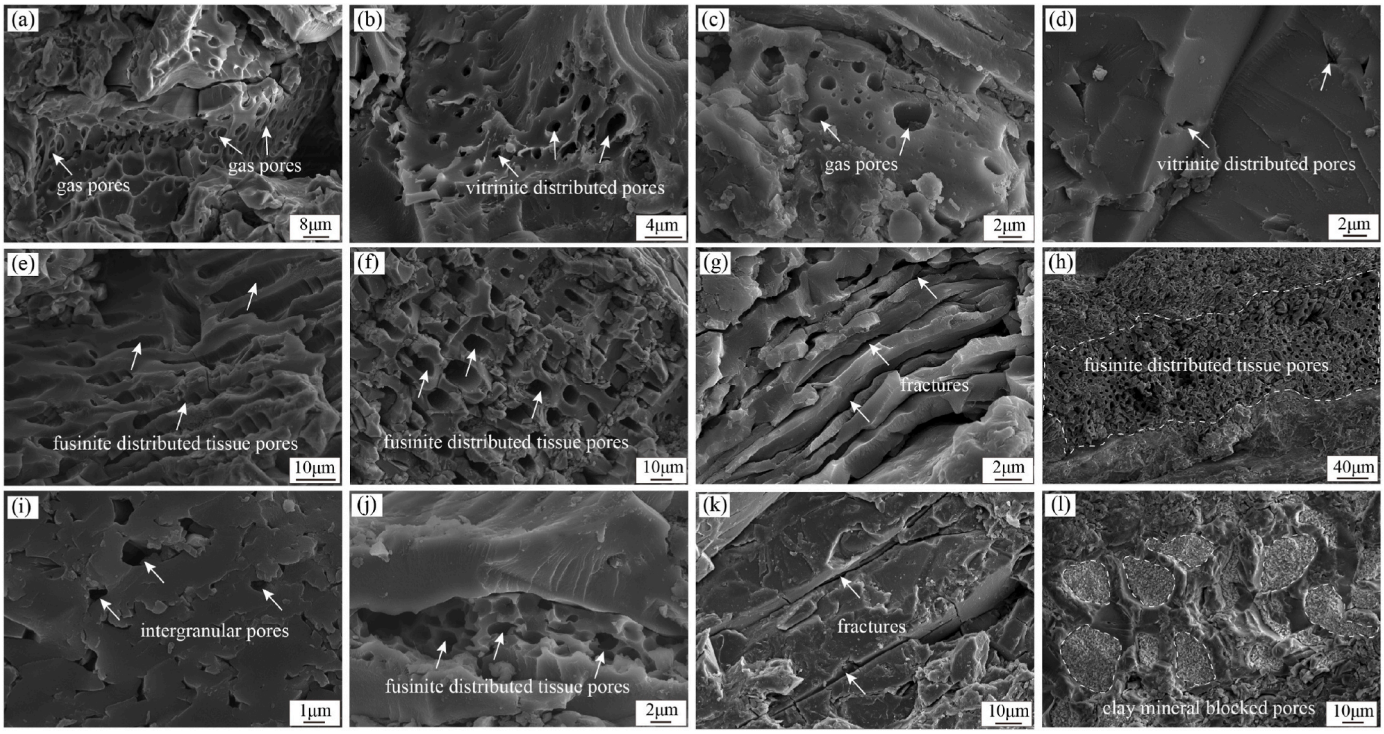

Fig. 11. SEM images of coal samples showing the various maceral pore development characteristics. **(a)** widely distributed gas pores; **(b)** homogeneous vitrinite distributed pores; **(c)** mass vitrinite distributed gas pores; **(d)** homogeneous vitrinite distributed pores; **(e)** fusinite widely distributed tissue pores; **(f)** fusinite widely distributed tissue pores; **(g)** fibrous fusinite distributed fractures and tissue pores; **(h)** fusinite widely distributed tissue pores; **(i)** intergranular pores of homogeneous vitrinite distributed; **(j)** fusinite widely distributed tissue pores; **(k)** fractures; **(l)** clay mineral (kaolinite) blocked pores.

variation of gas content in the T_1-T_2 map. Therefore, well log data will provide continuous evaluation of total gas content and industrial components. Actually, T_1 and T_2 spectrum from NMR logs has the advantages for characterizing coal gas content and pore structures [50].

5. Discussion

5.1. Comprehensive characterization of pore structure

The pore size distribution curves across various diameter ranges can be obtained through processing LP-CO_2GA, LT-N_2GA and MIP. The NLDFT and Washburn's model can be utilized to select the optimal pore size segments for each test method [24,51]. These curves are then integrated to offer a comprehensive quantitative description of the full-scale pore structure in low - medium rank coals (Fig. 10).

The PSD curves of low-medium rank coals indicate a bimodal distribution dominated by micropores and macropores, with limited mesopore development. (Fig. 10a and b). However, the PSD curves of certain samples (MQ2, MQ3) exhibit notable deviations from the T_2 spectrum of NMR, particularly within the pore size range of micropores and mesopores (Figs. 7 and 10b). This discrepancy stems from the smaller size of CO_2 molecules relative to water molecules. Additionally, differences between the two methods arise from variations in detection principles, sample preparation techniques, and molecular weight effects [11,12,14,24].

SSA curves analysis reveals the predominance of micropores in contributing to the total specific surface area. While PSD curves show variations among coal samples, they maintain similar distribution patterns, with micropores contributing comparable pore volumes to macropores (Fig. 10c). The SSA curves demonstrate minimal variation across samples, with micropores consistently dominating the SSA, consistent with previous research findings [4,8,9,51]. The significant contribution of micropores to both PV and SSA suggests that these micropores with high SSA the primary sites for CBM adsorption [2,47]. Consequently, a detailed investigation of micropore development and pore structure characteristics is essential.

The SEM images are observed of low-medium rank coal, and the cellular structure is typically well-preserved and exhibits a regular, oval shape. These cells predominantly form open pores, although they are occasionally filled with minerals. The surface structure exhibits a high

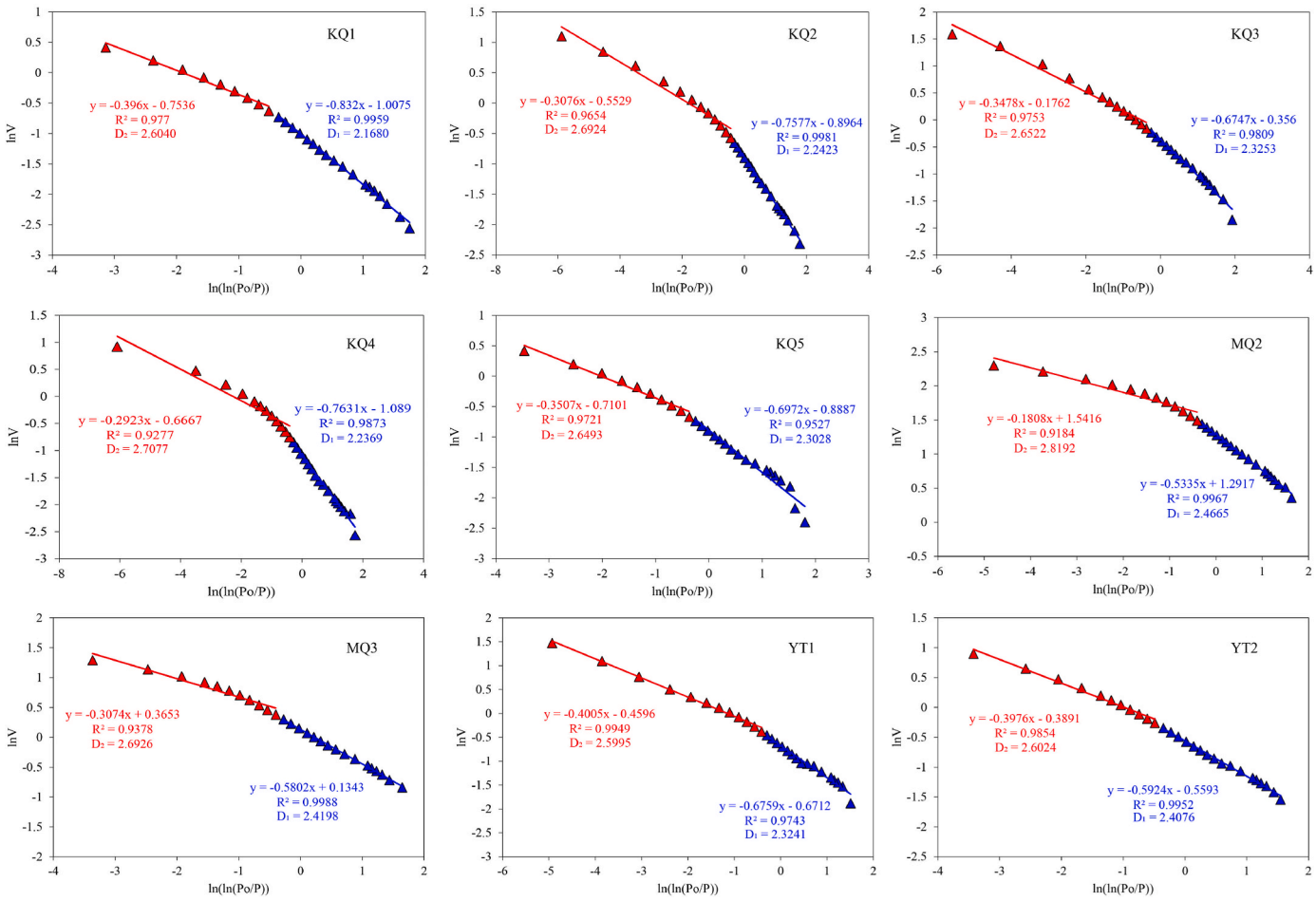

Fig. 12. Fractal characterization of pore distribution of coal samples by LT-N_2GA.

level of complexity and obvious heterogeneity (Fig. 11). Plant tissue pores, gas pores, intergranular pores of plant and fractures are development. It is clear that both homogeneous and mass vitrine are mainly involved in the development of gas pores (Fig. 11a, b, c, d). While pores in plant tissue pore mainly form in the inertinite (fusinite), numerous pores and fractures are also found (Fig. 11e, f, g, h). Compared to high-rank coal, low-medium rank coals contain a few gas pores, as significant gas generation has not yet commenced during this coalification stage (Fig. 11b, c, d) [19,36,47,52]. Additionally, kaolinite filling between plant fragments obstructs these pores (Fig. 11i). SEM observations reveal that the inertinite in low-medium rank coals exhibits extensive pore development with uneven size distribution.

5.2. *Fractal characterization from LT-N_2GA and NMR*

The coal exhibits pores of varying scales, indicating a complex pore structure and great heterogeneity. It is feasible to effectively characterize the multi-scale pore structure by integrating the methods of LT-N_2GAand NMR (Figs. 12 and 13). As is described in the FHH fractal model outlined in Section 2.2, the fractal dimensions D_1 and D_2 from LT -N_2GA data were utilized to calculate for the adsorption pores. The fractal dimension can be divided into two parts: one is controlled by monolayer and multilayer adsorption, and the other is affected by capillary condensation [3,4,22,45]. Fractal dimension D_1 ranges from 2.1680 to 2.4574, with an average value of 2.3393, while D_2 ranges from 2.5995 to 2.8192, with an average value of 2.6981 (Fig. 12). Overall, D_1 is slightly lower than D_2, which means that the complexity of pore structure grows as the pore size gets larger. Previous studies suggest that D_1 and D_2 may refer to the fractal dimensions of pore surface and pore structure, respectively [22,31,49]. A larger D_2 value reveals a complex heterogeneous structure in large pores [22].

The NMR results of the adsorption fractal dimension D_3 ($T_2 \leq 2.5$ ms) and seepage space fractal dimension D_4 ($T_2 > 2.5$ ms) varied from 0.9955 to 1.4815 and 2.7621–2.9854, with an average of 1.2165, 2.8775, respectively (Fig. 13). The significant differences observed in D_3 indicate noteworthy discrepancies in the adsorption characteristics among different coal samples. The increase of D_3 value results in heightened complex and irregularity of the adsorption pore surface, thereby giving rise to a more intricate internal surface structure that is conducive to methane adsorption [18,21,36]. In Fig. 11(a–c), abundant gas pores are observed, and the surfaces of the adsorption pores are irregular, indicating that greater pore-wall surface complexity will increase the D_3 value. Meanwhile, the increase in D_4 value indicates a greater complexity in the pore structure of seepage pores within coal samples, resulting in weakening connectivity [29,48,52]. In addition, abundant tissue pores and fractures are observed, indicating that g a higher permeability and a lower D_4 value.

Fig. 12 shows the relation of pore parameters to fractal dimension. We found a significant positive correlation between fractal dimension D_1 and the SSA, TPV of micropores and mesopores, respectively, indicating that rougher coal surfaces correspond to larger values of D_1 (Fig. 14). Additionally, D_2 exhibits a positive correlation with the SSA, TPV of micropores and mesopores, respectively (Fig. 14). This suggests that a more intricate pore structure corresponds to an increased SSA [19,51]. There exists a direct relationship between TPV and SSA, leading to a positive correlation (Fig. 2d) [7,16,21,47]. Consequently, it can be shown that the rise in the fractal dimension of low-medium rank coal is related to the roughness of the pore surface and the complexity of the

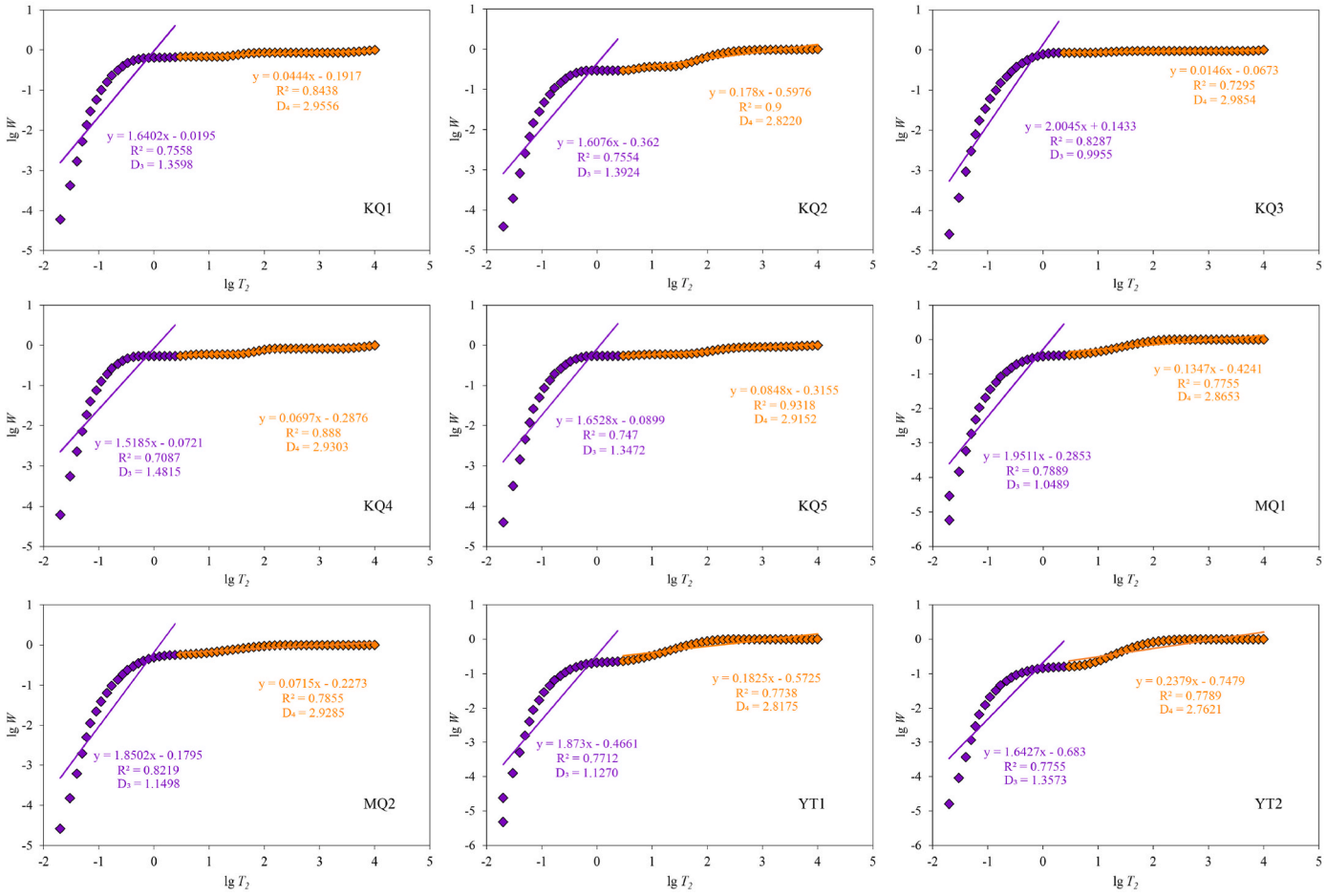

Fig. 13. Fractal characterization of pore distribution of coal samples by NMR.

pore structure [21,49,52].

5.3. Impact of pore structure on adsorbability and seepage

Langmuir volume (V_L) is a crucial parameter for assessing CBM resources, often used to assess CH_4 adsorption capacity of coal reservoirs [14,17,24]. Adsorbability of coal is influenced by complex geological factors, with pore structure playing a crucial role in the process [4,20,26]. A comprehensive analysis is conducted to investigate the impact of pore structure on the adsorption capabilities of low-medium rank coal. The CH_4 isothermal adsorption curves show significant variations (Fig. 15a).

The SSA of micropores and mesopores is negatively correlated with the V_L, indicating that increased SSA of micropores and mesopores does not enhance adsorption capacity (Fig. 15b and c). This suggests that adsorption theories for medium-high-rank coals may not fully apply to low-medium rank coals, necessitating further exploration of testing methods for the latter [47]. Additionally, a negative correlation between moisture content and V_L (Fig. 15d) was observed, indicating that moisture occupies adsorption sites in coal reservoirs, inhibiting methane adsorption. This may result from the greater presence of oxygen-containing functional groups (hydroxyl and carboxyl) in low-medium rank coals, which enhance hydrophilicity and reduce energy availability for methane adsorption [3,53].

In general, the pores size of adsorption is typically less than 100 nm, while pores with a pore size larger than 100 nm are mainly regarded as seepage pores [11,21,36]. There was no significant correlation between D_1 and V_L, but a positive correlation between D_3 and V_L (Fig. 16), suggesting that coal heterogeneity of pore surface affects gas adsorption capacity. Higher D_3 indicates the significant CBM adsorption capacity [11,21]. Macropores and microfractures influence coal permeability and are crucial for methane desorption and extraction [14,22]. Additionally, there is a significant negative correlation between D_4 and both saturation of movable fluid and permeability (Fig. 17), indicating that a smaller D_4 reflects a stronger pore connectivity, which enhances methane flow in coals [21,52].

5.4. Gas content of low-medium rank coal

The potential of coal resources is vast; however, there remains a need for comprehensive research on the impact of pore structure on gas content in deep low-medium rank coal [24,37,38]. In this study, logging data are utilized to calculate gas content and industrial components, and continuous T_1 and T_2 spectrum of coal seams were obtained through CMR-NG. (Figs. 9 and 18). Here, T_1 spectrum reflects the fluid information of coal, while T_2 spectrum represents the pore structure characteristics [54,55]. In the T_1–T_2 map, distinct signal regions are corresponded to different fluid types [50,54]. In coal seam 3 (Fig. 9), three energy clusters are observed at a depth of 4460.4 m: the low-energy cluster in the lower-left corner represents clay-bound water; the medium-energy cluster represents bound gas and partially bound water; and the high-energy cluster in the upper-right corner represents free gas residing in pores. In addition, at 4461.6 m only two energy clusters are present: the medium-energy cluster reflects bound gas residing in pores together with partially bound water, while the upper-right high-energy cluster is weak and close to the water line, which represents free water.

Fig. 18 illustrates the comprehensive logging response

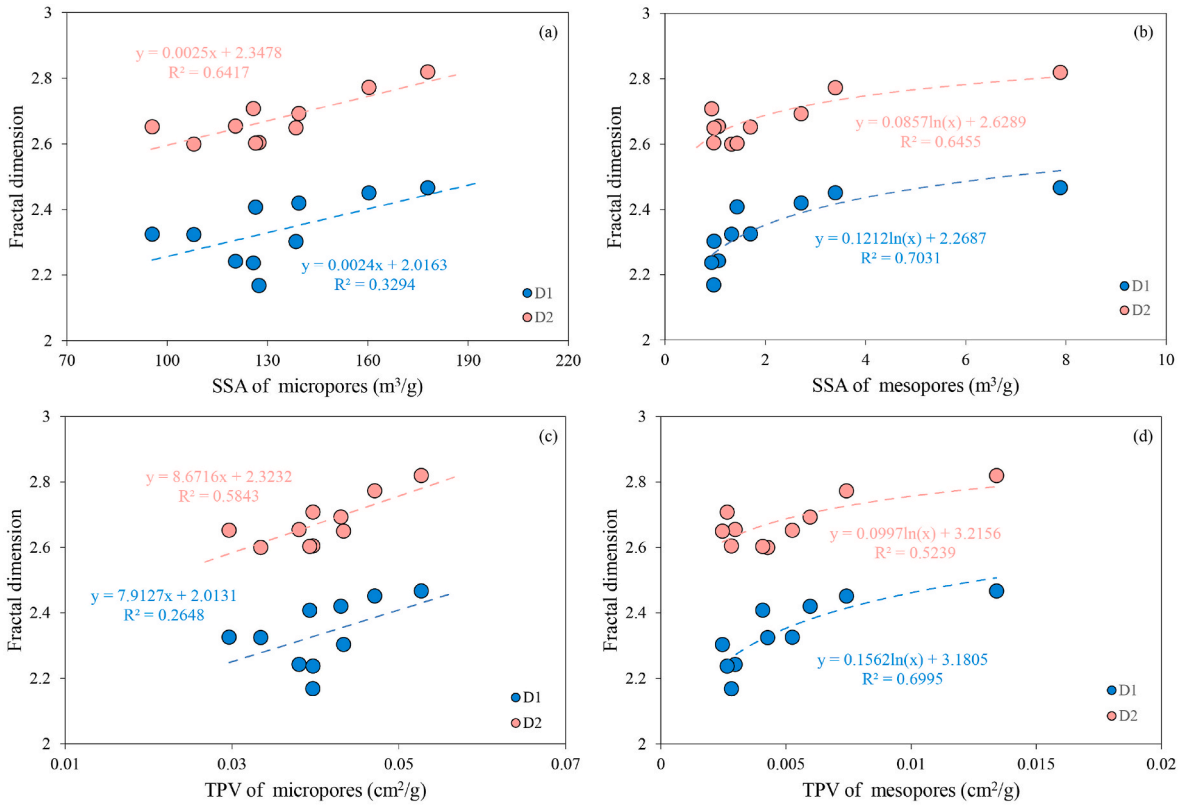

Fig. 14. The relationship between D_1 and D_2 with the SSA and TPV of micropores and mesopores, respectively.

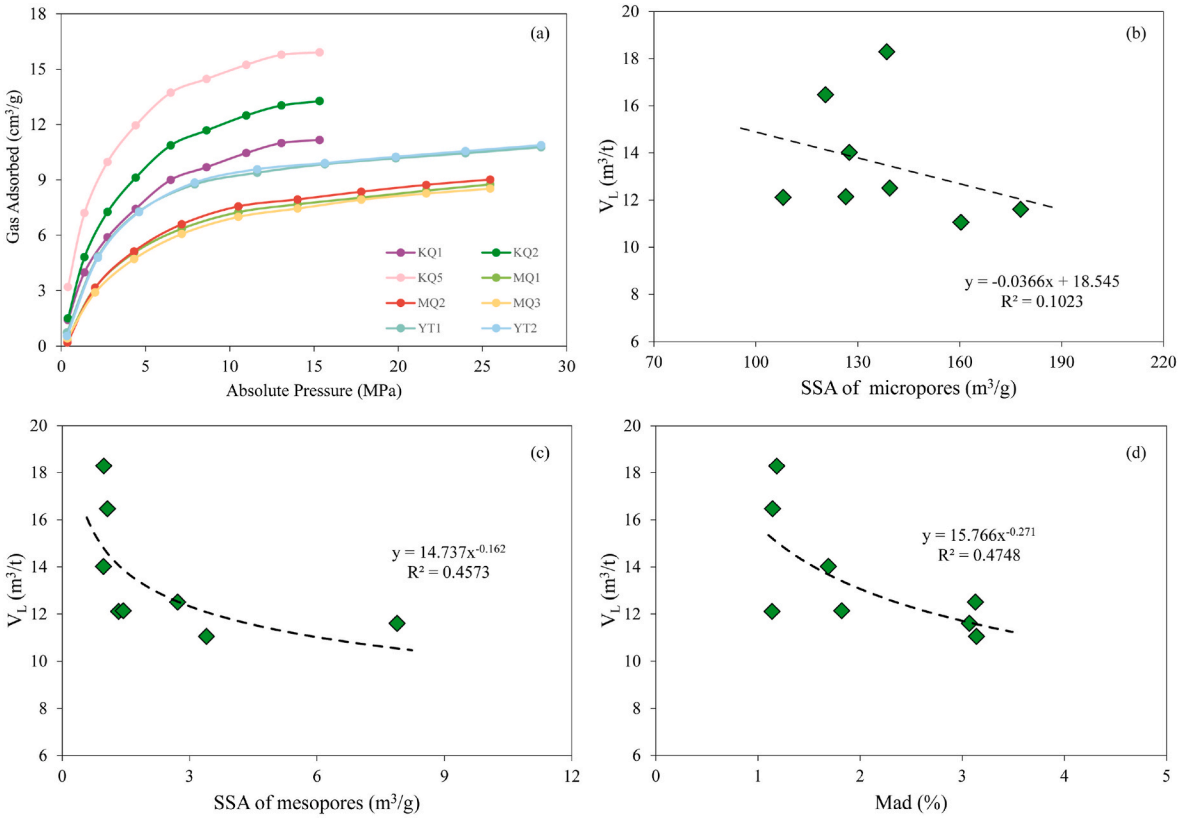

Fig. 15. Isothermal adsorption curves of coal samples, and the relationship between V_L and SSA of micropores, SSA of mesopores and Mad, respectively.

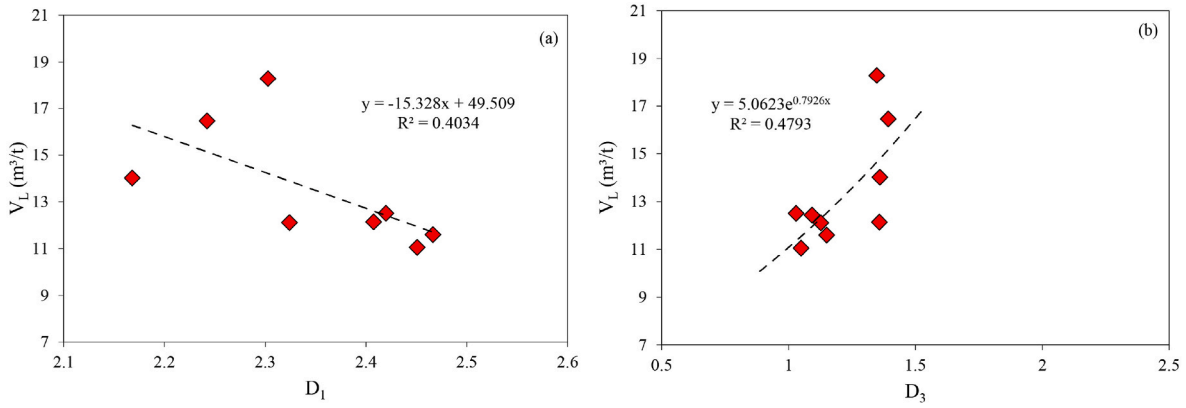

Fig. 16. The relationship between V_L and D_1, D_3, respectively.

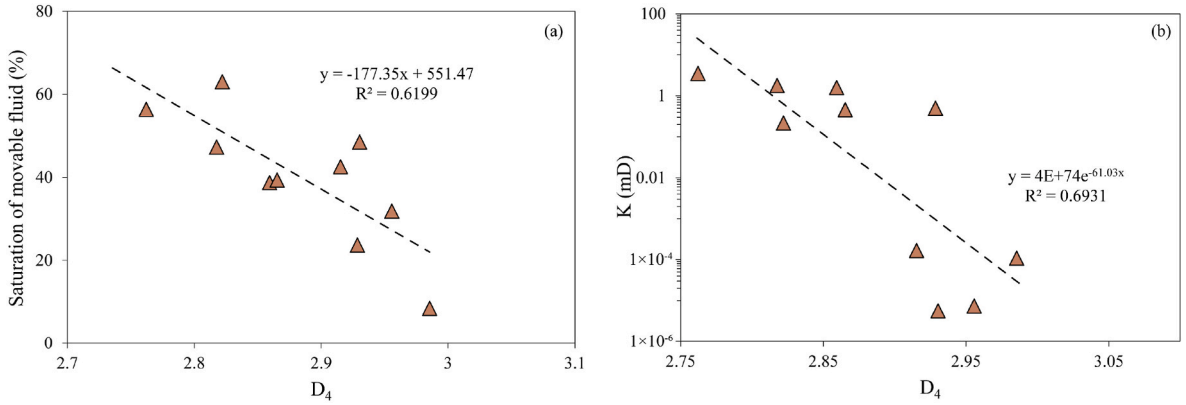

Fig. 17. The relationship between D_4 and saturation of movable fluid, K, respectively.

characteristics of coal seams, which exhibit high resistivity, high compensated neutron porosity, high acoustic transit time, low gamma ray as well as low bulk density compared to mudstone. Notably, significant differences in gas content are observed between Layer 1 and Layer 2, with layer 2 exhibiting higher gas content than layer 1 (Fig. 18). Furthermore, it is found that the resistivity log is often sensitive to changes in gas and remains consistent with changes in total gas content curve.

The T_1 and T_2 spectrum of CMR_NG in two layers exhibit significant differences. The T_2 spectrum of Layer 2 displays a bimodal feature with tail distribution, which shows that there are small pores as well as large pores in the coals. Whereas Layer 1 predominantly shows a single peak and left skewed, suggesting the abundance of small pores [50]. Additionally, there are variations in gas content, as evidenced by the T_1 spectrum displaying a single peak on the left for Layer 1, indicative of primarily adsorbed gas, which is further supported by the T_1-T_2 map (Fig. 18a). Conversely, the broader peak in the T_1 spectrum of Layer 2 suggests the existence of free gas within large pores and adsorbed gas within small pores, consistent with observations on the T_1-T_2 map where B and C contain both adsorbed and free gases, although with a certain amount of water signal among them. (Fig. 18b and (c)). Previous researches have demonstrated that deep coal seams contain both adsorbed and free gas [22,37].

Further analysis is conducted to investigate the controlling factors of gas content in deep coal seams. The calculated gas content from logging corresponds to variations in T_1 and T_2 spectrum, leading us to compare the measured total gas content at different sample depths with T_1LM (logarithmic mean of T_1 distribution) and T_2LM (logarithmic mean of T_2 distribution). It is found that both parameters exhibited a strong positive correlation (Fig. 19a and b), indicating that T_2LM and T_1LM control the pore structure of coal seams and their relevant gas content, respectively. Additionally, a significant positive association can be noticed between fixed carbon content and measured total gas content, while a strong negative correlation is observed between ash content and measured total gas content (Fig. 19c and d). The fixed carbon content curve of Layer 2 is significantly higher than that of Layer 1, which is consistent with the total gas content, while the ash content shows the opposite trend (Fig. 18). This suggests that fixed carbon provides a material basis for the development of pores in deep coal seams, whereas ash may block pores, hindering methane enrichment, consistent with previous findings [3,47].

In summary, the industrial components and pore structure of low-medium rank coal show a significant implication on their gas content. Fixed carbon contributes to increased adsorption and seepage space within coal reservoir, while ash content can obstruct pores and decrease permeability. Low-medium rank coal are predominantly characterized by micropores and macropores, as evidenced by bimodal or trimodal distribution in nuclear magnetic T_2 spectrum, primarily originating from plant tissue pores with a limited number of gas pores. In addition, a higher adsorption fractal dimension D_3 indicates better methane adsorption capacity in coal; conversely, a smaller D_4 improves pore connectivity and enhances permeability. The evaluation of coal reservoir of well YT1, coal seam 1 exhibits high total gas content, with a broad T_1 spectrum peak, and a bimodal T_2 spectrum indicating the presence of adsorbed and free gas, identifying it as the optimal coal reservoir.

6. Conclusion

The pore structure of coal samples in Kuqa Depression was

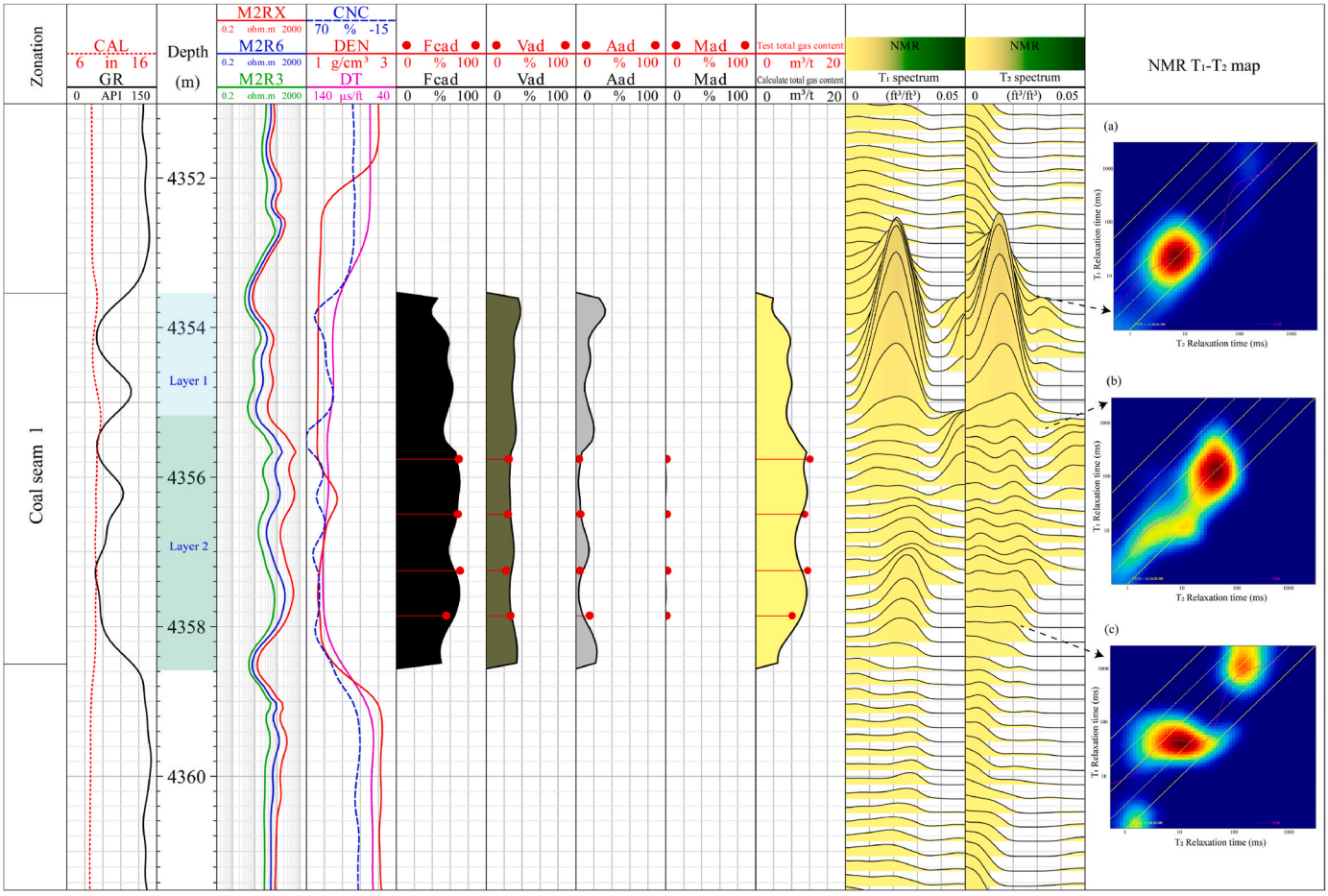

Fig. 18. Logging characteristics and NMR T_1-T_2 map of coal seam of Well YT 1 in Tarim Basin.

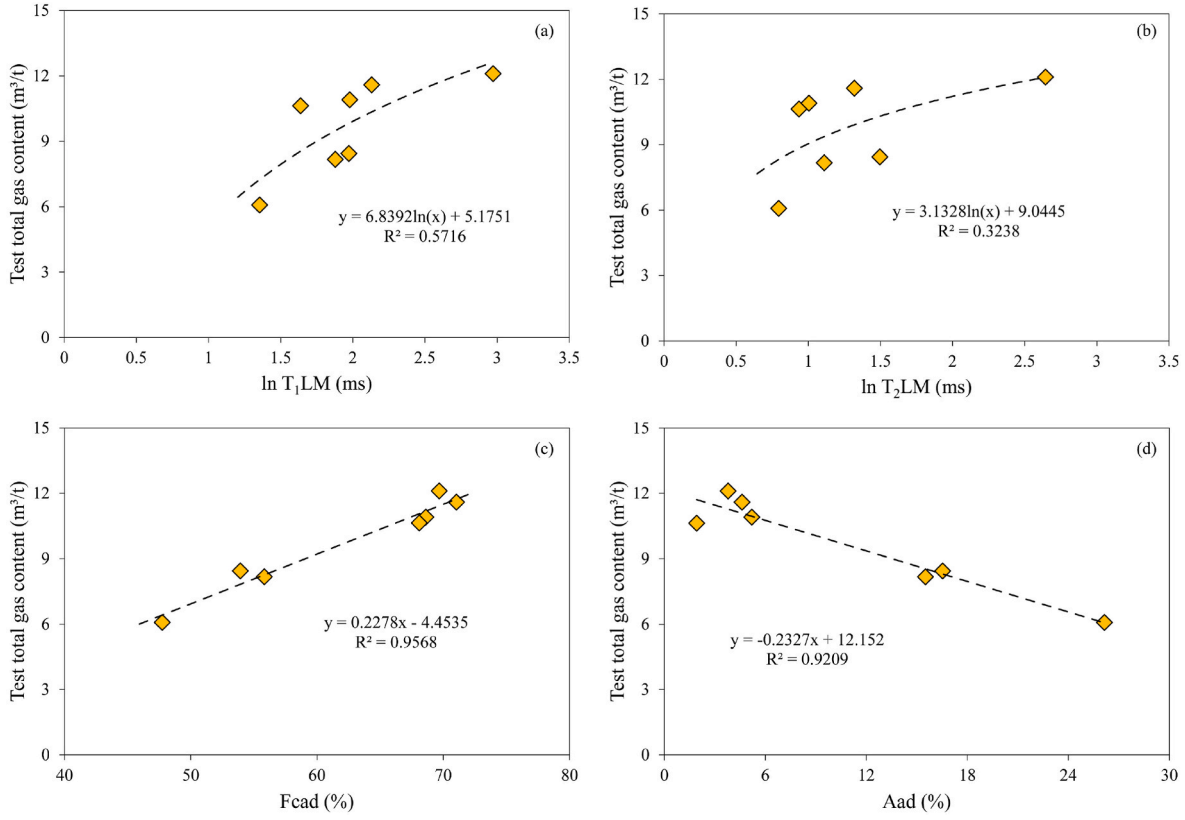

Fig. 19. The relationship between test total gas content and lnT_1LM, lnT_2LM, Fcad, Aad, respectively.

comprehensively characterized using LT-N_2GA, LP-CO_2GA, MIP, SEM, NMR techniques and well log data. A comparative analysis was also performed on the pore characteristics of low-medium rank coal. The conclusions are as follows.

(1) Low–medium-rank coals exhibit ink-bottle and narrow slit pores; pore systems are dominated by micropores and macropores, with limited mesopores. Micropores increase SSA but correlate weakly with CH_4 adsorption due to moisture; As moisture decreases, methane adsorption capacity improves.
(2) Micropore surface roughness and mesopore structural complexity enhance SSA and correlate positively with D_1 and D_2. CH_4 adsorption increases with D_3; while D_4 inversely indicates permeability (smaller D_4 implies better connectivity and higher permeability). The research results are important for a deeper understanding of the adsorption and seepage of coalbed methane.
(3) The gas content and distribution in deep coal are determined by the industrial components and pore structure. An increase in fixed carbon content can create more pores for methane adsorption, leading to higher gas content; however, ash content can block pores, hindering methane enrichment. A broad T_1 spectrum peak, and a bimodal T_2 spectrum indicates the presence of small pore adsorbed gas and large pore free gas in coal, while a left single peak T_1 and T_2 spectrum mainly reflects the existence of small pore adsorbed gas.

CRediT authorship contribution statement

Fei Zhao: Writing – original draft, Validation, Methodology, Investigation. **Jin Lai:** Writing – review & editing, Supervision, Formal analysis. **Lu Xiao:** Visualization, Supervision, Investigation. **Zongli Xia:** Supervision, Formal analysis, Data curation. **Zhongrui Wang:** Validation, Investigation, Formal analysis. **Ling Li:** Resources, Project administration, Data curation. **Bin Wang:** Resources, Project administration, Data curation. **Guiwen Wang:** Writing – review & editing, Resources, Project administration.

Declaration of competing interest

The authors declare that they have no known competing financial interests or personal relationships that could have appeared to influence the work reported in this paper.

Acknowledgements

This work is financially supported by Science Foundation of China University of Petroleum, Beijing (No.2462023QNXZ010) and Strategic cooperation project of PetroChina and CUPB (ZLZX2020-01). The authors thank PetroChina Tarim Oilfield Company for their data input to this work.

References

[1] G. Aydin, H. Jang, E. Topal, Energy consumption modeling using artificial neural networks: the case of the world's highest consumers, Energy Sources, Part B 11 (3) (2016) 212–219.
[2] Z. Wang, S. Li, Z. Jin, Z. Li, Q. Liu, K. Zhang, Oil and gas pathway to net-zero: review and outlook, Energy Str. Rev. 45 (2023) 101048.
[3] R.M. Bustin, C.R. Clarkson, Geological controls on coalbed methane reservoir capacity and gas content, Int. J. Coal Geol. 38 (1–2) (1998) 3–26.
[4] M. Mastalerz, A. Drobniak, D. Strąpoć, W. Acosta, S. Rupp, Variations in pore characteristics in high volatile bituminous coals: implications for coal bed gas content, Int. J. Coal Geol. 76 (3) (2008) 205–216.
[5] S. Tao, Z. Pan, S. Chen, S. Tang, Coal seam porosity and fracture heterogeneity of marcolithotypes in the fanzhuang block, southern qinshui basin, China, J. Nat. Gas Sci. Eng. 66 (2019) 148–158.
[6] T. Wang, F. Tian, Z. Deng, H. Hu, The characteristic development of micropores in deep coal and its relationship with adsorption capacity on the eastern margin of the ordos basin, China, Minerals 13 (3) (2023) 302.

[7] K. Mosher, J. He, Y. Liu, E. Rupp, J. Wilcox, Molecular simulation of methane adsorption in micro-and mesoporous carbons with applications to coal and gas shale systems, Int. J. Coal Geol. 109 (2013) 36–44.
[8] B. Hu, Y. Cheng, Z. Pan, Classification methods of pore structures in coal: a review and new insight, Gas Sci. Eng. 110 (2023) 204876.
[9] Y. Li, C. Zhang, D. Tang, Q. Gan, X. Niu, K. Wang, R. Shen, Coal pore size distributions controlled by the coalification process: an experimental study of coals from the junggar, ordos and qinshui basins in China, Fuel 206 (2017) 352–363.
[10] X. Du, Y. Cheng, Z. Liu, H. Yin, T. Wu, L. Huo, C. Shu, CO_2 and CH_4 adsorption on different rank coals: a thermodynamics study of surface potential, gibbs free energy change and entropy loss, Fuel 283 (2021) 118886.
[11] J. Zhao, H. Xu, D. Tang, J.P. Mathews, S. Li, S. Tao, A comparative evaluation of coal specific surface area by CO_2 and N_2 adsorption and its influence on CH_4 adsorption capacity at different pore sizes, Fuel 183 (2016) 420–431.
[12] S. Yu, J. Bo, F. Lan, Competitive adsorption of $CO_2/N_2/CH_4$ onto coal vitrinite macromolecular: effects of electrostatic interactions and oxygen functionalities, Fuel 235 (2019) 23–38.
[13] M. Thommes, K. Kaneko, A.V. Neimark, J.P. Olivier, F. Rodriguez-Reinoso, J. Rouquerol, K. Sing, Physisorption of gases, with special reference to the evaluation of surface area and pore size distribution (IUPAC technical report), Pure Appl. Chem. 87 (9–10) (2015) 1051–1069.
[14] D. Liu, F. Qiu, N. Liu, Y. Cai, Y. Guo, B. Zhao, Y. Qiu, Pore structure characterization and its significance for gas adsorption in coals: a comprehensive review, Unconv. Resour. 2 (2022) 139–157.
[15] T.A. Moore, Coalbed methane: a review, Int. J. Coal Geol. 101 (2012) 36–81.
[16] Y. Lin, Y. Qin, D. Ma, Z. Duan, Pore structure, adsorptivity and influencing factors of high-volatile bituminous coal rich in inertinite, Fuel 293 (2021) 120418.
[17] P.J. Crosdale, B.B. Beamish, M. Valix, Coalbed methane sorption related to coal composition, Int. J. Coal Geol. 35 (1–4) (1998) 147–158.
[18] J. Zhao, D. Tang, Y. Qin, H. Xu, Fractal characterization of pore structure for coal macrolithotypes in the hancheng area, southeastern ordos basin, China, J. Petrol. Sci. Eng. 178 (2019) 666–677.
[19] S. Liu, S. Sang, H. Liu, Q. Zhu, Growth characteristics and genetic types of pores and fractures in a high-rank coal reservoir of the southern qinshui basin, Ore Geol. Rev. 64 (2015) 140–151.
[20] Z. Meng, S. Liu, G. Li, Adsorption capacity, adsorption potential and surface free energy of different structure high rank coals, J. Petrol. Sci. Eng. 146 (2016) 856–865.
[21] Y. Yao, D. Liu, D. Tang, S. Tang, W. Huang, Z. Liu, Y. Che, Fractal characterization of seepage-pores of coals from China: an investigation on permeability of coals, Comput. Geosci. 35 (6) (2009) 1159–1166.
[22] S. Li, Y. Qin, D. Tang, J. Shen, J. Wang, S. Chen, A comprehensive review of deep coalbed methane and recent developments in China, Int. J. Coal Geol. 279 (2023) 104369.
[23] Z. Li, T. Ren, X. Li, M. Qiao, X. Yang, L. Tan, B. Nie, Multi-scale pore fractal characteristics of differently ranked coal and its impact on gas adsorption, Int. J. Mining Sci. Technol. 33 (4) (2023) 389–401.
[24] T. Wang, Z. Deng, H. Hu, R. Ding, F. Tian, T. Zhang, Z. Ma, D. Wang, Pore structure of deep coal of different ranks and its effect on coalbed methane adsorption, Int. J. Hydrogen Energy 59 (2024) 144–158.
[25] Z. Ma, S. Tao, L. Gao, Y. Cui, Q. Jing, S. Chen, W. He, J. Guo, L. Hai, Detailed characterization of microscopic pore structure in low-rank coal: a case study of zhalainuoer coalfield, Nat. Resour. Res. 33 (5) (2024) 2261–2277.
[26] J. Yan, Z. Meng, K. Zhang, H. Yao, H. Hao, Pore distribution characteristics of various rank coals matrix and their influences on gas adsorption, J. Petrol. Sci. Eng. 189 (2020) 107041.
[27] J. Lai, G. Wang, Z. Wang, J. Chen, X. Pang, S. Wang, Z. Zhou, Z. He, Z. Qin, X. Fan, A review on pore structure characterization in tight sandstones, Earth Sci. Rev. 177 (2018) 436–457.
[28] F. Wang, Y. Cheng, S. Lu, K. Jin, W. Zhao, Influence of coalification on the pore characteristics of middle–high rank coal, Energy Fuels 28 (9) (2014) 5729–5736.
[29] Y. Yao, D. Liu, Comparison of low-field NMR and mercury intrusion porosimetry in characterizing pore size distributions of coals, Fuel 95 (2012) 152–158.
[30] X. Wang, J. Pan, K. Wang, T. Ge, J. Wei, W. Wu, Characterizing the shape, size, and distribution heterogeneity of pore-fractures in high rank coal based on X-ray CT image analysis and mercury intrusion porosimetry, Fuel 282 (2020) 118754.
[31] Y. Yao, D. Liu, D. Tang, S. Tang, W. Huang, Fractal characterization of adsorption-pores of coals from north China: an investigation on CH_4 adsorption capacity of coals, Int. J. Coal Geol. 73 (1) (2008) 27–42.
[32] K. Bauer, J. Kulenkampff, J. Henninges, E. Spangenberg, Lithological control on gas hydrate saturation as revealed by signal classification of NMR logging data, J. Geophy. Res.: Solid Earth 120 (9) (2015) 6001–6017.
[33] J. Lai, G. Wang, Q. Fan, X. Pang, H. Li, F. Zhao, Y. Li, X. Zhao, Y. Zhao, Y. Huang, M. Bao, Z. Qin, Q. Wang, Geophysical well-log evaluation in the era of unconventional hydrocarbon resources: a review on current status and prospects, Surv. Geophy. 43 (3) (2022) 913–957.
[34] S. Yarmohammadi, A. Kadkhodaie, S. Hosseinzadeh, An integrated approach for heterogeneity analysis of carbonate reservoirs by using image log based porosity distributions, NMR T2 curves, velocity deviation log and petrographic studies: a case study from the south pars gas field, Persian gulf basin, J. Petrol. Sci. Eng. 192 (2020) 107283.
[35] X. Fu, Y. Qin, G.X. Wang, V. Rudolph, Evaluation of coal structure and permeability with the aid of geophysical logging technology, Fuel 88 (11) (2009) 2278–2285.
[36] B. Zhou, G. O'Brien, Improving coal quality estimation through multiple geophysical log analysis, Int. J. Coal Geol. 167 (2016) 75–92.
[37] C. Zou, Q. Zhao, H. Liu, et al., China's breakthrough in coal-rock gas and its significance, Nat. Gas. Ind. 45 (4) (2025) 1–18.
[38] G. Li, C. Jia, Q. Zhao, T. Zhou, J. Gao, Coal-rock gas accumulation mechanism and the whole petroleum system of coal measures, Petrol. Explor. Dev. 52 (1) (2025) 29–43.
[39] W. Ju, K. Wang, A preliminary study of the present-day in-situ stress state in the ahe tight gas reservoir, dibei gasfield, kuqa depression, Mar. Petrol. Geol. 96 (2018) 154–165.
[40] S. Guo, X. Lyu, Y. Zhang, Relationship between tight sandstone reservoir formation and hydrocarbon charging: a case study of a Jurassic reservoir in the eastern kuqa depression, tarim basin, NW China, J. Nat. Gas Sci. Eng. 52 (2018) 304–316.
[41] J. Wang, Y. Gong, W. Huang, Q. Zhuo, X. Lu, Characteristics of hydrocarbon migration and accumulation in the Lower Jurassic reservoirs in the tugerming area of the eastern kuqa depression, tarim basin, J. Petrol. Sci. Eng. 208 (2022) 109748.
[42] T. Gao, X. Ding, X. Yang, C. Chen, Z. Xu, K. Liu, X. Zhang, W. Cao, Geochemical characteristics and depositional environment of coal-measure hydrocarbon source rocks in the northern tectonic belt, kuqa depression, Appl Sci 12 (19) (2022) 9464.
[43] W. Huang, L. Zeng, C. Pan, Z. Xiao, H. Zhang, Z. Huang, Q. Zhao, S. Yu, H. Xu, C. Cheng, D. Liu, J. Liu, Petroleum generation potentials and kinetics of coaly source rocks in the kuqa depression of tarim basin, northwest China, Org. Geochem. 133 (2019) 32–52.
[44] J. Lai, F. Zhao, Z. Xia, Y. Su, C. Zhang, Y. Tian, G. Wang, Z. Qin. Well log prediction of total organic carbon: A comprehensive review. Earth-Science Rev 258 (2024) 104913.
[45] R. Evans, U.M.B. Marconi, P. Tarazona, Capillary condensation and adsorption in cylindrical and slit-like pores, J. Chem. Soc., Faraday Trans. 2 (10) (1986) 1763–1787, 82.
[46] D. Avnir, M. Jaroniec, An isotherm equation for adsorption on fractal surfaces of heterogeneous porous materials, Langmuir 5 (6) (1989) 1431–1433.
[47] S. Tao, S. Chen, D. Tang, X. Zhao, H. Xu, S. Li, Material composition, pore structure and adsorption capacity of low-rank coals around the first coalification jump: a case of eastern junggar basin, China, Fuel 211 (2018) 804–815.
[48] S. Chen, D. Tang, S. Tao, X. Ji, H. Xu, Fractal analysis of the dynamic variation in pore-fracture systems under the action of stress using a low-field NMR relaxation method: an experimental study of coals from Western Guizhou in China, J. Petrol. Sci. Eng. 173 (2019) 617–629.
[49] P. Ren, H. Xu, D. Tang, Y. Li, Z. Chen, C. Sun, F. Zhang, S. Chen, F. Xin, L. Cao, Pore structure and fractal characterization of main coal-bearing synclines in Western Guizhou, China, J. Nat. Gas Sci. Eng. 63 (2019) 58–69.
[50] V. Anand, M.R. Ali, N. Al-Adani, D. Willis, R. Freedman, F. Hamichi, A. Grover, R. Abubaker, O. Neto, J. Iglesias, New generation NMR tool for robust, continuous T1 and T2 measurements, in: SPWLA Annual Logging Symposium, SPWLA, 2015. SPWLA.
[51] D. Song, X. Ji, Y. Li, H. Zhao, B. Song, K. He, Heterogeneous development of micropores in medium-high rank coal and its relationship with adsorption capacity, Int. J. Coal Geol. 226 (2020) 103497.
[52] H. Fu, D. Tang, T. Xu, H. Xu, S. Tao, S. Li, Z. Yin, B. Chen, C. Zhang, L. Wang, Characteristics of pore structure and fractal dimension of low-rank coal: a case study of Lower Jurassic xishanyao coal in the southern junggar basin, NW China, Fuel 193 (2017) 254–264.
[53] H. Fu, D. Tang, H. Xu, S. Tao, T. Xu, B. Chen, Z. Yin, Abrupt changes in reservoir properties of low-rank coal and its control factors for methane adsorbability, Energy Fuels 30 (3) (2016) 2084–2094.
[54] S. Wang, G. Wang, L. Huang, L. Song, Y. Zhang, D. Li, Y. Huang, Logging evaluation of lamina structure and reservoir quality in shale oil reservoir of fengcheng formation in mahu sag, China, Mar. Petrol. Geol. 133 (2021) 105299.
[55] Y. Huang, G. Wang, Y. Zhang, J. Xi, L. Huang, S. Wang, Y. Zhang, J. Lai, C. Jiang, Logging evaluation of pore structure and reservoir quality in shale oil reservoir: the fengcheng formation in mahu sag, junggar basin, China, Mar. Petrol. Geol. 156 (2023) 106454.